EFFICIENCY IMPROVEMENTS WITH LOW HEAT REJECTION CONCEPTS APPLIED TO LOW TEMPERATURE COMBUSTION

A Thesis

by

MICHAEL ABRAHAM PENNY

Submitted to the Office of Graduate and Professional Studies of
Texas A&M University
in partial fulfillment of the requirements for the degree of

MASTER OF SCIENCE

Chair of Committee,	Timothy Jacobs
Committee Members,	Jerald Caton
	Adonios Karpetis
Head of Department,	Andreas Polycarpou

August 2014

Major Subject: Mechanical Engineering

ABSTRACT

With increasingly stringent governmental regulations on engine emissions such as oxides of nitrogen (NO_X) and particulate matter (PM), there is a strong motivation to decrease the production and release of these harmful substances from internal combustion engines. Simultaneously, there are on-going efforts to increase fuel efficiency to curb usage of natural resources and emission of carbon. In general, improvements in one of these areas comes at the cost of the other; however, the results of a previous computational study have indicated that emissions can be decreased while simultaneously increasing efficiency through the application of low heat rejection (LHR) techniques to low temperature combustion (LTC). The goal of this study is to experimentally confirm these findings using a light duty, multi-cylinder diesel engine. LTC is realized through high levels of exhaust gas recirculation (EGR) and retarded injection timings while different degrees of LHR are achieved by means of higher coolant temperatures which should serve to decrease the temperature gradients across the cylinder walls. An energy balance is conducted on the engine to ensure the validity of the efficiency findings.

By applying LHR techniques to LTC operation, the undesirable side effects of LTC were found to be mitigated. Specifically, the emissions of carbon monoxide (CO) and unburned hydrocarbons (HC) were reduced and the loss in engine efficiency was also diminished. NO_X and PM emissions did increase but they remained at acceptably low levels. In addition, the results of the energy balance substantiated these trends by properly accounting for the bulk of the input energy. While the full potential of improvements in LTC were not explored due to current engine limitations, these results point to the viability of further research into LHR-LTC concepts.

DEDICATION

To Kathleen and my family, who have encouraged me all along the way.

ACKNOWLEDGEMENTS

Special thanks to the many people who have helped me along the way including my family, teachers, advisor, Dr. Jacobs, and committee members, Dr. Caton and Dr. Karpetis.

Also, thanks to those who have helped make this work possible. The preparation of this study is based on work funded by the National Science Foundation through grant #1247290. Any opinions or views expressed in this manuscript are not necessarily those of the sponsoring agency.

TABLE OF CONTENTS

Page

ABSTRACT ii

DEDICATION iii

ACKNOWLEDGEMENTS iv

TABLE OF CONTENTS v

LIST OF FIGURES vii

LIST OF TABLES ix

1. INTRODUCTION 1

    1.1. Motivation 1
    1.2. Background 2
        1.2.1. NOx Formation 2
        1.2.2. Particulate Matter Formation 3
    1.3. Objective 5

2. LITERATURE REVIEW 7

    2.1. Low Temperature Combustion 7
        2.1.1. HCCI 7
        2.1.2. PCCI 8
        2.1.3. RCCI 9
        2.1.4. Control Parameters 9
    2.2. Low Heat Rejection 10
    2.3. Coolant Temperature Effects 11

3. EXPERIMENTAL SETUP AND METHODOLOGY 13

    3.1. Engine and Controller 13
    3.2. Fuel 14
    3.3. Measurements and Data Acquisition 15
        3.3.1. Stock Sensors 15
        3.3.2. In-Cylinder Pressure 15
        3.3.3. Surface Temperatures 15
        3.3.4. Auxiliary Sensors 16
        3.3.5. Calibration, Uncertainty, and Miscellaneous Information 18
    3.4. Experimental Test Matrix 18
        3.4.1. LTC Characterization 18
        3.4.2. Application of LHR to LTC Operation 20
    3.5. Calculations 21
        3.5.1. Exhaust Gas Recirculation 21

Page

3.5.2. Apparent Heat Release Rate 23
3.5.3. System Energy Balance 25
3.5.4. Fuel Energy 26
3.5.5. Intake Air Energy 27
3.5.6. Exhaust Energy 28
3.5.7. Brake Power 28
3.5.8. Coolant Heat Transfer 29
3.5.9. Charge Air Heat Transfer 29
3.5.10. Surface Heat Transfer 30
3.5.11. Remainder of Energy 32
3.5.12. Energy Balance Uncertainty 32
3.5.13. Brake Specific NO_X Emissions 32
3.5.14. Efficiencies 33
3.6. Parameter Summary 34

4. RESULTS AND DISCUSSION 35

4.1. LTC Characterization 35
4.1.1. Objective 35
4.1.2. NO_x and PM Emissions 35
4.1.3. Supplementary Trends 40
4.1.4. Discussion 44
4.2. LHR-LTC Operation 45
4.2.1. Objective 45
4.2.2. NO_X and PM Emissions 45
4.2.3. Pressure and AHRR Trends 51
4.2.4. CO and HC Emissions 53
4.2.5. Efficiencies 54
4.2.6. Energy Balance 58
4.2.7. Summary of Important Results 66
4.2.8. Discussion 66

5. SUMMARY AND CONCLUSIONS 68

REFERENCES 70

APPENDIX A 74

APPENDIX B 75

LIST OF FIGURES

Page

Figure 1. Effect of temperature on forward rate coefficient of first Zeldovich reaction 3

Figure 2. Effects of temperature on formation and oxidation rates of soot in diesel fuel [8] 4

Figure 3. NOX and soot concentrations as functions of equivalence ratio and temperature, adapted from [9] 5

Figure 4. Annotated infrared image of engine coolant pipe 16

Figure 5. Diagram of engine cylinder depicting various work and energy terms 24

Figure 6. Diagram of engine depicting various mass and energy fluxes 25

Figure 7. Exhaust concentrations of NOX (left) and filter smoke number (right) as a function of injection timing and EGR level 36

Figure 8. NOx concentration as a function of smoke number for three injection timings and three EGR levels. 37

Figure 9. NOx concentration as a function of smoke number for both days of data 38

Figure 10. Brake specific NOX emissions as a function of injection timing and EGR level 39

Figure 11. Relative reduction in BSNOX as a function of injection timing and EGR level 40

Figure 12. In-cylinder pressure (left) and AHRR (right) as a function of engine operation 41

Figure 13. Exhaust concentrations of CO (left) and HC (right) as a function of injection timing and EGR level 42

Figure 14. Combustion efficiency as a function of injection timing and EGR level 43

Figure 15. Brake fuel conversion efficiency as a function of injection timing and EGR level 44

Figure 16. Exhaust concentrations of NOX as a function of ECT 46

Figure 17. Brake specific NO_X emissions as a function of ECT 48

Figure 18. Relative reduction in $BSNO_X$ for LTC conditions as a function of ECT 49

Figure 19. Filter smoke number as a function of ECT 50

Page

Figure 20. In-cylinder pressure (left) and AHRR (right) for conventional combustion as a function of ECT 51

Figure 21. In-cylinder pressure (left) and AHRR (right) for LTC as a function of ECT 52

Figure 22. Exhaust concentrations of CO (left) and HC (right) as a function of ECT 53

Figure 23. Combustion efficiency as a function of ECT 54

Figure 24. Brake thermal conversion efficiency as a function of ECT 56

Figure 25. Brake fuel conversion efficiency as a function of ECT 57

Figure 26. Unaccounted percentage of input energy as a function of ECT 58

Figure 27. Percentage of input energy rejected through coolant as a function of ECT 59

Figure 28. Percentage of input energy for brake work as a function of ECT 61

Figure 29. Percentage of input energy exiting in exhaust as a function of ECT 62

Figure 30. Post-turbocharger exhaust temperatures as a function of ECT 62

Figure 31. Percentage of input energy in sensible enthalpy of the exhaust as a function of ECT 63

Figure 32. Percentage of input energy rejected by surface heat transfer as a function of ECT 64

Figure 33. Percentage of input energy rejected by intercooler as a function of ECT 65

LIST OF TABLES

Page

Table 1. Specifications of the light-duty engine apparatus under investigation 13
Table 2. Summary of the properties of the fuel used in this study.....14
Table 3. Specifications of Horiba emission testing equipment.....17
Table 4. LTC test matrix 20
Table 5. LHR-LTC test matrix.....21
Table 6. Definition of cylinder energy balance terms.....24
Table 7. Definition of engine energy balance terms 26
Table 8. Characteristic length for each surface.....31
Table 9. Measurement and calculation methods summary 34
Table 10. Comparison of maximum and minimum NOX values 46
Table 11. Change in LTC measurements due to increase of ECT to 100°C.....66
Table 12. Total uncertainty of energy balance for conventional combustion.....74
Table 13. Total uncertainty of energy balance for LTC.....74
Table 14. Conventional combustion energy balance terms for Day 1 75
Table 15. Conventional combustion energy balance terms for Day 2 75
Table 16. LTC energy balance terms for Day 1.....76
Table 17. LTC energy balance terms for Day 2.....76

1. INTRODUCTION

1.1. Motivation

Since the first of its kind sputtered to life over a hundred years ago, internal combustion engines have undergone numerous advancements and improvements. Through the ingenuity and imagination of inventors and engineers, technological innovations such as carburetors and turbochargers have been developed to enhance their performance. In the early years, much of the work was dedicated to increasing the horsepower or power density of the engines, but in the last several decades, there has been an increased focus on reducing both fuel consumption and exhaust emissions. One of the major driving forces behind this movement is government regulations that have decreased the amount of pollutants that can be exhausted by engines [1]. Particularly, the allowable exhaust levels of pollutants such as oxides of nitrogen (NO_X), particulate matter (PM), and carbon dioxide (CO_2) have been significantly tightened. Simultaneously, there are on-going efforts to increase fuel efficiency to curb usage of natural resources and emission of carbon.

To meet these increasingly stringent fuel efficiency and emissions standards, a number of engine improvements are being explored, particularly advanced combustion techniques and exhaust after-treatment devices. As the name suggests, exhaust treatment entails the filtration or catalysis of product gases, liquids, and solids after exiting the engine to eliminate undesirable emissions. In general, these methods focus solely on meeting emissions standards, and often come at the cost of reduced engine efficiency. In contrast, advanced combustion strategies seek to prevent the formation of pollutants by directly altering the behavior of the reaction within the cylinder. One promising field of study is the pursuit of low temperature combustion (LTC) techniques. Through the reduction of in-cylinder temperatures, these LTC methods have been shown to reduce emissions such as PM and NO_X [2]. Of course, these improvements come at the cost of increasing other pollutants such as carbon monoxide (CO) and hydrocarbon (HC) emissions [2].

Another promising field of interest is the concept of an "adiabatic" engine, more accurately described as a low heat rejection (LHR) engine. Through means such as insulating the cylinder walls, heat transfer to the engine block can be reduced, resulting in less useful energy being lost to the environment [3, 4]. Since more energy remains contained, theoretically more work can be extracted from the mixture by the piston, thereby increasing the efficiency of the engine [3, 4]. In addition, LHR engines tend to require smaller cooling systems, resulting in lower parasitic losses on the engine to accessories like water pumps.

1.2. Background

1.2.1. NOx Formation

During the combustion of fuels that do not contain significant levels of nitrogen, such as gasoline and diesel, NO_X can be formed by any of four known mechanisms from the nitrogen contained in air: Zeldovich, Fenimore, N_2O intermediate, and NNH. At the elevated temperatures typical of internal combustion engines, the extended Zeldovich mechanism dominates the formation of NO_X pollutants as found in a computational study [5]. This mechanism can be defined by essentially three elementary reactions [6].

$$O + N_2 \leftrightarrow NO + N \quad (1)$$

$$N + O_2 \leftrightarrow NO + O \quad (2)$$

$$N + OH \leftrightarrow NO + H \quad (3)$$

The first reaction, which initiates the mechanism, possesses a large activation energy of 319,050 kJ/kmol, that results in a strong temperature dependence [7]. Consequently, it progresses very slowly at lower temperatures which in turn slows the rate of the whole mechanism. To better illustrate the response of NO_X formation to temperature change, the following plot of temperature's effect on the mechanism is shown in Figure 1.

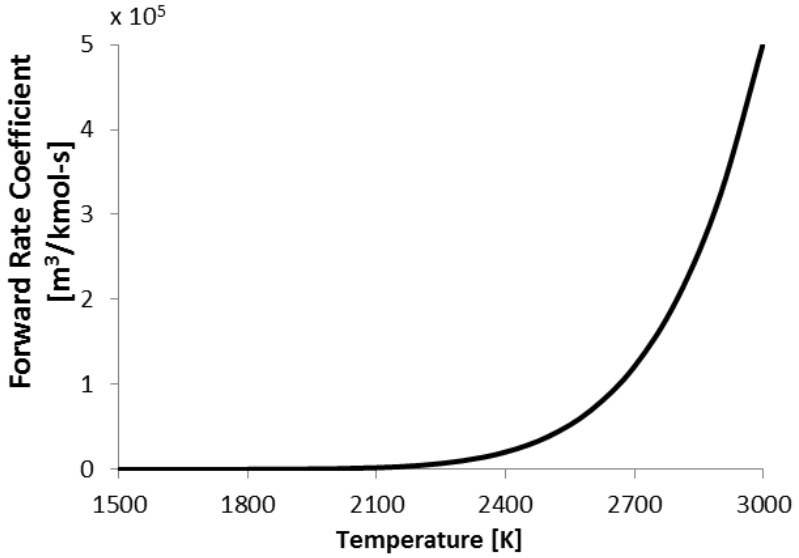

Figure 1. Effect of temperature on forward rate coefficient of first Zeldovich reaction

As readily apparent, by decreasing the peak temperature within an engine's operating cycle, the rate of NO_X formation driven by the Zeldovich mechanism can be drastically reduced. In fact, at temperatures below 1800 K, the pollutants created by this mechanism become negligibly small and are largely unaffected by further reductions in temperature [7].

1.2.2. Particulate Matter Formation

The formation of PM is another substantial concern during the combustion of fuels such as diesel, with carbonaceous material (soot) making up a significant portion of particulate emissions in diesel engines [6]. Like NO_X formation, the net release of carbonaceous soot is also dependent temperature. Put extremely simply, at fuel-lean equivalence ratios, more oxygen is available relative to the amount of fuel and soot, allowing for a greater percentage of soot to completely oxidize before exiting the reaction zone. The reverse is true at rich equivalence ratios. In addition, like most reactions, soot formation and oxidation are strongly dependent on temperature. The

effect of temperature on the rates of soot formation and oxidation for a constant equivalence ratio are illustrated in Figure 2.

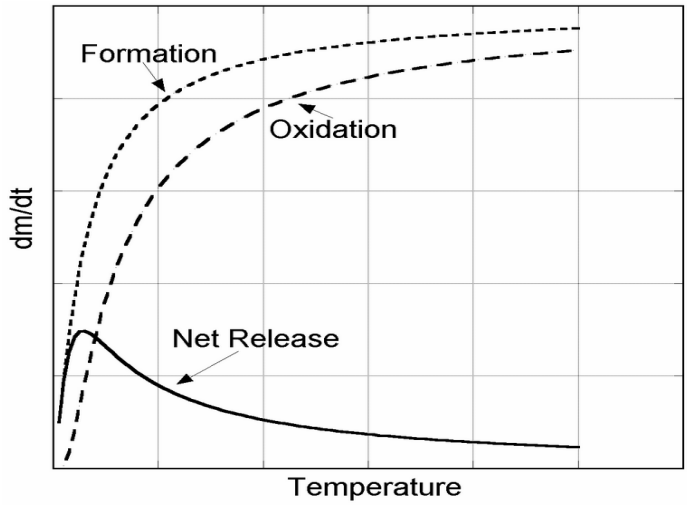

Figure 2. Effects of temperature on formation and oxidation rates of soot in diesel fuel [8]

While higher chamber temperatures increase both the rate of soot formation and oxidation, the rate of soot oxidation begins to converge on the rate of soot formation. This relative difference between the two rates determines how much soot will be emitted as a pollutant, yielding the reduced net release of soot seen at higher temperatures of Figure 2.

The contrary effects of changing the reaction temperature on both NO_X and soot formation has been termed the "NO_X-soot tradeoff," where modifications to the normal combustion behavior of diesel engines improve the emissions behavior of one pollutant at the expense of another [7]. Despite this apparent dilemma, the extreme left portion of Figure 2 actually shows a decrease in soot emissions caused by the inability of soot to form at low temperatures. In this combustion regime, one can simultaneously reduce the formation of NO_X and soot without any tradeoff between the two. The combined effects of the local equivalence ratio and temperature on pollutant concentrations, along with the region of low temperature combustion, are shown in Figure 3.

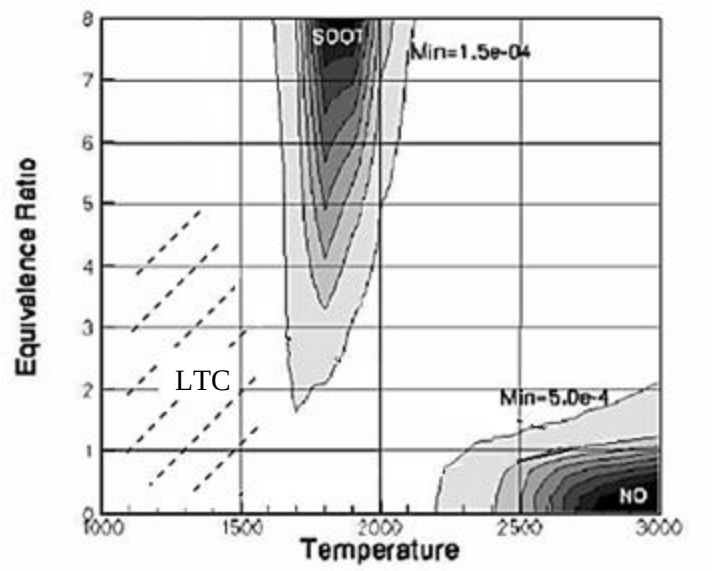

Figure 3. NO_X and soot concentrations as functions of equivalence ratio and temperature, adapted from [9]

For diesel engines, most of the combustion occurs at temperatures and equivalence ratios that intersect both regions of pollutant formation, but by decreasing the reaction temperature to the LTC area shown in Figure 3, the regions where NO_X and soot are formed can be both largely avoided regardless of the local equivalence ratio.

1.3. Objective

Based upon the results of previous studies, it has been proposed to investigate experimentally a combination of LTC and LHR concepts. It is thought that reducing the overall combustion temperature through LTC techniques will result in a ratio of specific heats which will more effectively convert the additional energy contained in-cylinder by LHR methods, compared to conventional combustion with LHR. Therefore, instead of only raising the thermal energy of the exhaust, more of the increased energy would be converted into work. In addition, the high NO_X emissions that appear in LHR engines would be reduced when used in conjunction with LTC methods. A computational study by Caton of such an LTC-LHR combination has predicted improvements in both emissions and efficiency [10]. Specifically, the brake thermal efficiencies of the LTC-

LHR hybrid were predicted to be approximately 10% higher than a conventional LHR engine under various levels of heat rejection. In addition, NO_X emissions for the LTC-LHR engine were predicted to be negligible. In this particular study, no corresponding experimental work was conducted to validate the results, and no specific LTC technique, e.g. HCCI, was cited as being used, just that the conditions in the cylinder were such that LTC was achieved.

Consequently, the objective of this current study is to experimentally confirm the results of the simulation study. This is a multi-phase effort and the first task to accomplish is to develop a suitable LTC mode. Upon confirmation of LTC operation, LHR concepts will be applied to the engine during conventional and LTC conditions to form comparisons between the two.

2. LITERATURE REVIEW

2.1. Low Temperature Combustion

Within the area of LTC, there are three major methods or techniques: Homogenous Charge Compression Ignition (HCCI), Premixed Charge Compression Ignition (PCCI) and Reactivity Controlled Compression Ignition (RCCI). Each of these strategies achieves LTC through different means and therefore has its own unique benefits and drawbacks.

2.1.1. HCCI

HCCI operation involves the ignition of a well-mixed charge simultaneously throughout the cylinder strictly using compression. Typically the fuel is port-fuel injected and inducted into the cylinder, resulting in a homogeneous fuel-air mixture within the cylinder [10]. Rather than burning with a well-defined reaction zone either stationary or moving, like conventional compression ignition (CI) or spark ignition (SI), all parts of the mixture combust as soon as they reach the auto-ignition point for the fuel, which typically occurs at a lower temperature than conventional reaction zones in CI or SI [10, 11]. The lean nature of the HCCI mixture also aids in lowering in-cylinder temperatures. As expected from this lower temperature, NO_X and soot emissions are greatly reduced [10, 12, 13]. In addition, since a flame does not need to propagate through the mixture, HCCI combustion proceeds very rapidly, therefore approaching the ideal constant-volume combustion. This behavior combined with the fuel-lean mixtures tends to lead to higher thermal efficiencies [10, 11]. As a drawback, it has been shown that CO and HC emissions increase during HCCI as a result of incomplete combustion and decreased oxidation in the exhaust [9, 14]. Additionally, fuel efficiency can actually drop if the issue of incomplete combustion is not managed properly [9, 10]. The most difficult hurdle to overcome, however, is the control of the actual ignition point of the fuel in the cylinder. Since there is not one single dominate factor like spark or injection timing to dictate when combustion begins, numerous factors affect the auto-ignition of

the air-fuel mixture and must all be controlled to achieve the proper timing of combustion [10]. In addition, HCCI has a limited load operating range because it is constrained on higher end by the maximum pressure rise rate set by the engine structure and on the lower end by the lean flammability limit of the air-fuel mixture [9].

2.1.2. PCCI

PCCI is similar to HCCI in that it attempts to achieve the simultaneous compression ignition of the air-fuel mixture at multiple points in the cylinder, but it differs in that the mixture is not truly homogenous and tends to be stratified in nature. Additionally, PCCI controls the ignition point of the fuel through different means, i.e. typically by altering when fuel is introduced into the cylinder [10, 15]. Fuel, usually diesel, is either injected earlier or later in the compression stroke than for conventional combustion. In the case of the early injection, the air-fuel mixture is allowed to more fully mix before being ignited by compression. Alternatively, if the fuel is injected near or at top dead center (TDC) and ignition delay is increased through various means such as the use of exhaust gas recirculation (EGR), combustion does not begin until after the injection is finished, and the fuel is allowed more time to become well-mixed [10, 15]. Because of this extended mixing period, both of these methods tend to eliminate the slower diffusion-limited portion of diesel combustion, resulting in rapid combustion and similar emission and efficiency benefits to HCCI. Similar to HCCI, PCCI also tends to suffer from high HC and CO emissions due to the altered combustion phasing in the cycle [15]. In addition, due to the long delay between injection and ignition, there is a major concern with the fuel jet impinging on the cylinder walls which can significantly decrease fuel efficiency and increase HC emissions [9, 15]. However, it has been shown that this concern can be mitigated through the implementation of a low-penetration fuel injector [15]. Lastly, PCCI is also restricted to low load conditions because it is difficult to introduce the higher levels of EGR needed to delay the combustion process for high load operation [9].

2.1.3. RCCI

Last but not least, RCCI involves the in-cylinder mixing of two fuels with dissimilar reactivities [16, 17]. Typically, a low reactivity fuel such as gasoline is port-fuel injected and inducted into the cylinder, and then a high reactivity fuel like diesel is directly injected in the cylinder. By varying the reactivity of the total mixture, the ignition point can be better controlled within the cycle. In addition, due to the increased variability of volatility and reactivity, multiple load conditions can be handled by this method unlike HCCI or PCCI. Initial tests on a single-cylinder diesel engine have indicated NO_X and soot emissions below the 2010 emissions standards as well as approximately 50% thermal efficiency [16]. Tests on a multi-cylinder engine showed similar low emissions and slightly lower thermal efficiency [17]. Unfortunately, this method also produces much higher HC and CO emissions than conventional diesel, up to four to ten times in some tests [17]. There has also been some question of the feasibility of a dual-fuel vehicle, but research is already progressing to answer this concern, e.g. the use of a cetane additive for gasoline rather than a separate fuel such as diesel [18].

2.1.4. Control Parameters

To assist in the control of the previously mentioned combustion methods, numerous engine parameters can be altered to achieve LTC. One of the more extensively implemented methods is alteration of the EGR level in the engine, appearing in numerous studies [2, 9, 14, 19]. The bulk of product gases that are introduced back into the cylinder through the EGR system do not participate in the combustion reaction, but instead act as a heat sink to absorb thermal energy [6, 7]. The peak temperature within the cylinder is reduced by this heat absorption, and the regions of NO_X and soot formation are better avoided as previously described. For maximum benefit from this method, the exhaust gases must be cooled prior to their reintroduction into the cylinder; otherwise, the hot exhaust will increase the intake air temperature and therefore the peak temperature within the engine cycle [7, 20]. One restriction of using EGR is the high levels often required by LTC methods, in some cases over 60%. These high levels limit

the amount of combustible air-fuel mixture allowed in the cylinder and as a result can restrict LTC techniques to part load conditions.

2.2. Low Heat Rejection

Since the 1980s, there have been numerous and extensive studies in exploring LHR engines. These studies basically fall into two categories: simulation and experimentation, and the results have been varied and even contradictory. Across the board, computational investigations have predicted improvements in the thermal efficiency of a LHR engine in the range of 4% to 12% over a conventional engine [3, 4]. Typically, the degree of improvement is based heavily on the assumptions and what type of engine used as the basis, i.e. naturally aspirated vs. turbocharged vs. turbocompounded. However, these estimates have been called by several to be oversimplified and inaccurate, particularly in the areas of heat transfer and combustion [3]. One group goes as far as to say that "the in-cylinder heat transfer characteristics of LHR engine are still not clearly understood." [4] As a result, these simulations tend to be overly optimistic and have yet to be fully reproduced by experimentation.

As for the experimental studies, the results are extremely inconsistent. Some experiments have shown marginal to appreciable improvements in thermal efficiency [21-24], but others have shown mixed results [25] or even degradation of efficiency [26, 27]. Some of this inconsistency can be attributed to the numerous means by which the studies reduced heat rejection. Most of the studies coated cylinder surfaces with similar ceramic materials whose lower thermal conductivities would have increased the thermal resistance of the cylinder walls; however, the material and thickness of the ceramic coating and degree to which the cylinder was insulated varied significantly. In addition, some of the experiments also altered or eliminated the coolant flow for certain cylinder surfaces [21, 26] to reduce the heat transfer by decreasing the driving temperature gradient. As an added complication, the compression ratio of the LHR engine was altered in some cases from the conventional engine thanks to the changes in cylinder geometry due to the ceramic coatings. This variation of multiple parameters seems to

contribute to the inconsistent results and makes comparisons between them incredibly difficult, if not impossible.

In addition to this variation, due to the lower heat transfer losses, LHR engines experience higher in-cylinder temperatures at which the ratio of specific heats of the mixture is less conducive to extracting work during expansion. As a result, even if more energy is being retained in the cylinder by lower heat transfer, most of this exits the cylinder in the form of increased exhaust energy rather than increased useful work [28]. This lower utility of available energy may explain why LHR engines only experience small efficiency gains if any at all. As a side note, the higher exhaust energy can be utilized by devices such as catalytic converters or turbochargers to improve the emissions or efficiency of the engine in other ways, but operation of these devices naturally involve inefficiencies of their own.

Furthermore, due to the higher in-cylinder temperatures, NO_X emissions from LHR engines tend be higher [4]. As would be expected from the "NO_X-soot trade-off" of conventional combustion, particulate emissions are generally lower, and unlike LTC methods, HC and CO emissions tend also to be lower [4].

2.3. Coolant Temperature Effects

Several studies have studied the effect of altering engine coolant temperature (ECT) on the energy balance of the engine [29, 30]. In general, brake power increased and coolant heat rejection decreased with elevated ECTs. The effect on brake power was significant, increasing it 14% relative to the baseline for a 20°C temperature increase in one case [30]. Coolant heat rejection rate was less sensitive to ECT, decreasing only 7% for the same temperature change. Interestingly, low load conditions were found to be more sensitive to changes in ECT, which bodes well for an application of these techniques to the low load conditions typical of LTC.

As for the other energy fluxes out of the engine, one study found that the exhaust enthalpy remained relatively constant [29] while the other found an increase in exhaust losses [30]. However, for the study that found an increase, EGR rate and boost levels

were not held constant, resulting in variations in exhaust temperatures and flow rates that call into question the validity of this increase. For the study that considered heat transfer from the surface of the engine, this parameter also increased as a function of ECT.

The effect of coolant temperature on NO_X emissions has been studied in conjunction with injection timing and EGR rate [31]. While ECT was found to have a less significant effect than the other two, it was not negligible, representing a 16% change in NO_X emissions at light load conditions. Similar to its effect on brake power, NO_X emission rates were more sensitive to ECT changes at low load operation. The corresponding effect of ECT variation on PM emissions has not been studied, but it is hypothesized that it should exhibit an opposite response to ECT, thanks to the NO_X-soot tradeoff typical of diesels.

3. EXPERIMENTAL SETUP AND METHODOLOGY

3.1. Engine and Controller

The test engine for this study is a four-cylinder light-duty diesel engine; the specifications of which are listed in Table 1. Of particular interest are some of the technologies that allow this study to be undertaken, such as a high pressure common rail fuel system with electronically controlled injection times, cooled EGR, and a variable geometry turbocharger. In addition, several other sensors and controls, discussed in more depth in Section 3.3.4, have been added to measure or control different aspects of the engine.

Table 1. Specifications of the light-duty engine apparatus under investigation

Parameter	Value
Bore	82 mm
Stroke	90.4 mm
Displacement	1.91 L
Rated Power	110 kW at 4000 rev/min
Rated Torque	315 N-m at 2000-2750 rev/min
Compression Ratio	18:1 (nominal)
Fuel System	High pressure common rail
Pump	Mechanically driven
Injection	Electronic, direct injection
Air System	Turbocharged intake with EGR
Turbocharger	Variable geometry

To operate the engine, this study utilizes a third-party controller that permits the real-time monitoring and control of virtually every sensor and valve on the engine, including the non-stock equipment. Of particular interest to this study are the control of the EGR valve position, fuel injection timings and duration, the common rail fuel pressure, and radiator fan speeds. Also embedded in the system are numerous PID

controllers to maintain a constant value for the numerous parameters that define an operating point. Finally, engine speed is controlled by a DC electric dynamometer (dyno) while engine load is controlled by the injection pulse width (fuel delivery rate).

3.2. Fuel

The fuel used in the test is standard Diesel #2 from a single barrel. While the fuel was from this particular barrel was not tested, its properties, given in Table 2, are similar to those which were used in a previous study at Texas A&M University [32].

Table 2. Summary of the properties of the fuel used in this study

Property	**Units**	**Value**[a]
Density	kg/m3	825.5
Net heat value	MJ/kg	43.008
Gross heat value	MJ/kg	45.853
Sulfur	Ppm	5.3
Viscosity	cSt	2.247
Cetane Number	--	51.3
Hydrogen	%-mass	13.41
Carbon	%-mass	85.81
Oxygen	%-mass	0.78
Initial boiling point	°C	173.4
Final boiling point	°C	340.5

[a] Measured or Calculated by Southwest Research Institute (San Antonio, Texas)

3.3. Measurements and Data Acquisition

3.3.1. Stock Sensors

Proper analysis of this study requires numerous measurements throughout the many primary and secondary systems of the test stand. The engine has a number of stock sensors and controls that are used by the original equipment manufacturer (OEM) to operate the engine. The control and output data of this equipment are integrated into the National Instruments (NI) data acquisition (DAQ) system and LabVIEW-based engine controller.

3.3.2. In-Cylinder Pressure

In-cylinder pressure is measured within each of the engine's cylinders on a crank-angle resolved basis using a piezo-electric pressure transducer installed in each of the glow plug ports. In order to correlate this data to the engine's position, an optical encoder with a resolution of 0.2 crank-angle degrees is installed on the front flywheel of the crankshaft. These transducers are calibrated before installation, and periodic fidelity checks are performed to ensure proper operations, e.g. fine adjustments during motoring to ensure alignment of transducers and encoder. To more accurately measure the steady state pressure profiles, these pressure measurements are collected for 200 consecutive cycles for each cylinder and ensemble averaged to minimize the effect of cycle-to-cycle variation.

3.3.3. Surface Temperatures

To measure the surface temperatures of the engine, images of the engine are captured on all sides by an infrared camera. Since the temperature measurements from the camera depend on the emissivity of the surface and ambient temperature in the room, a thermocouple is used to probe the surface temperatures in key areas as well as the ambient conditions. The emissivity parameter of the camera is then adjusted until the temperatures match. This process is repeated for each distinctive type of surface, e.g. the oxidized steel of the exhaust manifold, the black plastic covers, and the painted rubber of the coolant hoses. Assuming that the emissivity of the surface remains

relatively constant, the temperature at various points on the surface are estimated using the provided software, producing images like Figure 4.

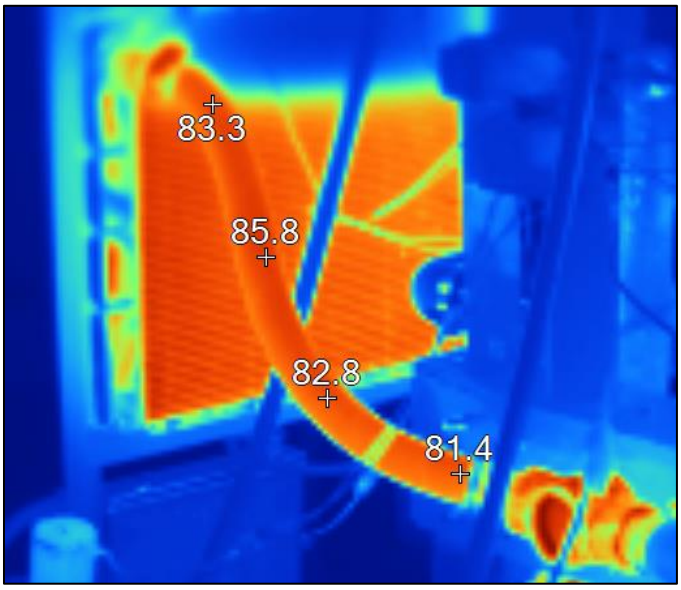

Figure 4. Annotated infrared image of engine coolant pipe

While the accuracy of these readings is naturally lower due to the numerous variables involved (e.g. changes in emissivity due to viewing angle or surface roughness), it is much more time effective than numerous surface mounted temperature probes, allowing rapid collection of entire surfaces of the engine. In addition, this level of inaccuracy is acceptable, considering that the similitude methods used to calculate the heat transfer from the surfaces, detailed in Section 3.5.10, contain intrinsic relative errors on the order of fifteen to twenty percent [33].

3.3.4. Auxiliary Sensors

To further augment the previously listed equipment, numerous sensors and regulators are added to the engine, most of which monitor the mass and energy exchanged between the engine and the surrounding environment.

To measure the air and fuel supplied to the engine, a laminar flow element (LFE) in the air intake and a positive displacement meter in the fuel supply system measure their respective flow rates. On the output side, the dyno contains a load cell to measure the brake torque, and a Horiba emission bench samples the composition of the exhaust. The specific exhaust species that are measured and the techniques used for the measurement are found in Table 3.

Table 3. Specifications of Horiba emission testing equipment

Species	**Technique of Measurement**
NO_x	Chemiluminescence
CO	Non-dispersive infrared
CO_2	Non-dispersive infrared
Total Hydrocarbons	Flame ionization detection
Smoke	Reflective smokemeter

The various cooling mediums for the engine comprise the remaining major modes of energy exchange. Foremost of these cooling fluids is the engine coolant which is circulated through the engine block, oil cooler and radiator. High-precision platinum resistance temperature detectors (RTDs) are installed in the coolant loop immediately upstream and downstream of the radiator to measure the temperature drop through it. These RTDs are calibrated using a dry block temperature calibrator. Additionally, a turbine flow meter is located between the engine and radiator with the necessary lengths of straight pipe before and after it in order to accurately determine the volumetric flow rate of the coolant. These measurements, coupled with tabulated data on the density and specific heat of the water-ethylene glycol mixture used as coolant [34], allows the heat rejection by the coolant to be calculated, the specifics of which are discussed in the Section 3.5.7.

In addition to the main coolant loop, the intake air is cooled post-compressor by an air-water heat exchanger, often commonly referred to as an "intercooler" but more correctly designated as a charge air cooler. Due to water's greater heat capacity relative to air, the temperature change of the air is more substantial and therefore more easily and accurately measured. When this temperature drop is combined with the intake air flow rate from the LFE and the tabulated enthalpies of air, calculation of heat rejected to the water is possible. The specifics of these calculations are found in Section 3.5.7.

3.3.5. Calibration, Uncertainty, and Miscellaneous Information

In addition to the calibrations previously mentioned, routine checks and adjustments are conducted to reduce systematic uncertainty. Furthermore, testing is conducted on multiple days to ensure the repeatability of the results. This multi-day data collection is imperative due to the numerous effects of ambient factors, namely air temperature and humidity, which can significantly affect parameters such as emissions and engine power output. Using standard statistical analysis techniques, the error bars in all data figures are created from these two data sets [35]. Lastly, any connecting lines within data figures are intended to assist in designating a single data set, not necessarily a trend between data points.

3.4. Experimental Test Matrix

3.4.1. LTC Characterization

Since this is the first LTC study to be conducted on this particular engine, a sweep of injection timings and EGR levels are needed to determine the test conditions necessary to achieve LTC using PCCI techniques. Using the EGR control valve, the EGR level is set to three values: a minimum (0%), an intermediate (~18%), and a maximum (~35%). In all subsequent plots, these three levels are referred to as "NoEGR", "MidEGR" and "MaxEGR", respectively. To achieve the intermediate and maximum values, the turbocharger is adjusted to its full boost position to provide the back pressure required to drive these higher levels. Due to numerous factors, particularly the manifold pressures, the EGR level does not necessarily remain constant for the same

control valve position. Therefore, the control valve is slightly adjusted for each set point to ensure a consistent EGR level.

For each EGR level, the injection timing is adjusted among three values, starting from the earliest position before moving to the intermediate and late timings. Between each timing setting, the engine is allowed to reach steady state before moving to the next test condition. To establish that the engine has actually reached a steady state, the coolant heat rejection rate and several temperatures around the engine (exhaust, coolant, etc.) are monitored until relatively constant values are observed for all parameters. Based on previous work conducted in the laboratory on a medium duty diesel engine, a "conventional" timing of 8° bTDC (crank angle degrees before top dead center) and a late timing of 1.5° bTDC are chosen. For the sake of establishing a trend between these two points, an intermediate timing of 4° bTDC is also included.

Initially, a late timing of 0° bTDC was chosen; however, during exploratory testing, combustion using this injection timing became extremely unstable at the maximum EGR level, causing the engine to misfire. Therefore, the timing was advanced until stable combustion could be reproduced at 1.5° bTDC, and this value was used as the late timing value for all EGR levels.

The engine is maintained at an operating speed of 1500 revolutions per minute (RPM) and a low load of condition of 30 N-m, which is equivalent to approximately 2 bar brake mean effective pressure (BMEP). The fuel rail pressure is held constant at 425 bar (which is approximately the factory calibrated setting for this speed and load condition) and injection duration is slightly adjusted (±2% of default value) to maintain the output load. The ECT is held constant at 90 °C throughout all points. For clarity, the testing conditions are summarized in Table 4.

Table 4. LTC test matrix

Control Parameters	Units	Values
EGR	%	0, 18, 35
Injection timing	°bTDC	1.5, 4, 8
Constant Parameters	**Units**	**Value**
Speed	RPM	1500
Engine load	N-m	30
BMEP	bar	2
Rail Pressure	bar	425
Injection duration	ms	~0.74

In addition, the order of test points is randomized within datasets as well as across sequential days to minimize any possible effects of testing procedures. If for some reason progressing from point A to B to C influences engine operation, this effect is minimized by collecting data in "B, C, A" order one day and "C, B, A" order on the next.

3.4.2. Application of LHR to LTC Operation

With the test conditions necessary for LTC identified, two operating points are chosen, namely the "conventional" timing of 8° bTDC with no EGR and the late timing of 1.5° bTDC with the engine's maximum EGR level. For each condition, the coolant temperature is varied among five values up to a maximum value of 100 °C. For the LTC operation, the lowest coolant temperature (75 °C) is limited by combustion instabilities while that of the conventional operation (56.5 °C) is limited by the amount of heat that can be rejected into the environment.

The engine is again maintained at a speed of 1500 RPM, a rail pressure of 425 bar, and an injection duration required to produce the 2 bar BMEP at an ECT of 90 °C. In contrast to the LTC characterization study, the injection duration is held constant throughout the test points to maintain a constant fueling rate to the engine. As a side note, while higher coolant temperatures would be desirable to accentuate any effects on

emissions or efficiency, the engine remains unmodified for high temperatures and extended operation at elevated temperatures would likely result in serious damage to components. This information is condensed for clarity in Table 5.

Table 5. LHR-LTC test matrix

Control Parameters	**Units**	**Values**
ECT	°C	--
Conventional	″	56.5, 65, 75, 90, 100
LTC	″	75, 82.5, 90, 95, 100
Constant Parameters	**Units**	**Value**
Injection timing	°bTDC	--
Conventional	″	8
LTC	″	1.5
EGR level	%	--
Conventional	″	0
LTC	″	35
Speed	RPM	1500
Engine load	N-m	30
BMEP	bar	2
Rail Pressure	bar	425
Injection duration	ms	0.74

3.5. Calculations

3.5.1. Exhaust Gas Recirculation

EGR level is regulated through control of the EGR valve position, i.e. it is opened a certain percentage. However, the correlation of this valve position to a mass percent of EGR is highly non-linear in nature due to the geometry of the mechanism. In addition, other engine parameters such as the intake and exhaust manifold pressures have significant but undocumented effects on the amount of EGR. Consequently, the EGR

level is calculated from emissions data, specifically the concentration of carbon dioxide (CO_2) in the intake manifold and the concentrations of the major exhaust species.

For this study, this calculation is based on a fairly standard procedure put forth by Heywood [6]. From an emissions standpoint, the EGR level is defined as the mass fraction of exhaust species in the intake,

$$EGR\% = \sum X_{intake,i} \tag{4}$$

where $X_{intake,i}$ is the mass fraction of each exhaust species in the intake.

The exhaust composition is measured on a molar (volume) concentration basis; however, some exhaust gases are measured on a dehumidified (dry) basis because water vapor interferes with the measurement techniques. Therefore, all the measured molar fractions are first converted to a wet basis,

$$Y_{i,wet} = \left(1 - Y_{H_20}\right) Y_{i,dry} \tag{5}$$

Though water concentration in the exhaust is not directly measured, its value is estimated by assuming equilibrium conditions for the water-gas shift reaction,

$$CO_2 + H_2 \leftrightarrow CO + H_2O \tag{6}$$

which has an associated empirical equilibrium constant, K. Choosing this constant to be 3.8 as recommended by Stivender [36], the following equation allows the molar fraction of water vapor to be calculated,

$$Y_{H_2O} = \frac{Y_{CO} + Y_{CO_2}}{2 \cdot r_{H/C}\left(1 + \frac{Y_{CO}}{K \cdot Y_{CO_2}}\right) + Y_{CO} + Y_{CO_2}} \tag{7}$$

where $r_{H/C}$ is the molar hydrogen-carbon ratio (H/C) of the fuel and the molar fractions of CO and CO_2 are the measured dry molar concentrations. As a side note, this relation assumes that the hydrocarbons in the exhaust are the same composition as the input fuel, which is not extremely accurate [37]; however, this assumption greatly simplifies the analysis.

With the molar concentration of water known, the true molar fractions of all the species are calculated in the exhaust. From this the mass fraction of the species are calculated,

$$X_i = \frac{Y_i \, MW_i}{MW_{mix,exh}} \tag{8}$$

where Y_i is the molar fraction of the exhaust gas, MW_i is the molecular weight of the gas, and $MW_{mix,exh}$ is the mixture average molecular weight of the exhaust gases which is calculated using the following relation,

$$MW_{mix,exh} = \sum_{i=1}^{mix} Y_i \, MW_i \tag{9}$$

Lastly, the molar concentration of CO_2 is measured downstream of the mixing of EGR and intake air to establish a dilution ratio, which allows the calculation of the mass fraction of each exhaust gas in the intake,

$$X_{intake,i} = \frac{Y_{CO_2,intake}}{Y_{CO_2,exhaust}} (X_i) \tag{10}$$

where $Y_{CO_2,intake}$ is the measured molar concentration after mixing, and $Y_{CO_2,exhaust}$ is the measured molar concentration in the exhaust. These mass fractions calculated from the dilution ratio of CO_2 finally allows the EGR level to be calculated using Eqn. (4).

3.5.2. Apparent Heat Release Rate

Using the in-cylinder pressure and known geometry of the piston-cylinder system, the apparent heat release rate (AHHR) of the combustion of fuel in the cylinder is estimated based on numerous assumptions. This heat release rate is used as an indicator of the rate at which the fuel burns in the cylinder and provides additional insight into the behavior of the combustion process.

The basis of the calculation is an energy balance performed on the gases trapped in the cylinder during compression, combustion, and expansion as shown in Figure 5,

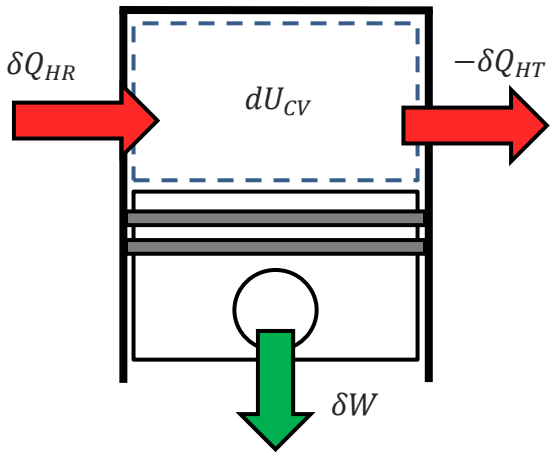

Figure 5. Diagram of engine cylinder depicting various work and energy terms

This depiction of the cylinder results in the following energy balance,

$$\delta Q_{HR} = \delta W + dU_{CV} + \delta Q_{HT} \tag{11}$$

where Table 6 defines the above terms,

Table 6. Definition of cylinder energy balance terms

Term	Definition
δQ_{HR}	Apparent heat release rate by fuel combustion
δW	Work extracted by piston
dU_{CV}	Internal energy of gases
δQ_{HT}	Heat rejected through cylinder wall

All of the terms aside from the AHHR are estimated from the measured parameters and established correlations and used to evaluate the AHHR. The specifics of the calculation of each term are not crucial for this study and have been derived and explained in depth elsewhere [38, 39]. In addition, the validity of this calculation has been demonstrated by other studies [38, 40, 41]. However, it is important to note that

the AHHR obtained is qualitative in nature due to the numerous assumptions embedded in its calculation, and it serves only as a comparison metric between testing conditions.

3.5.3. System Energy Balance

To perform an energy balance on the engine, a control volume must be created around the entire engine, through which mass and energy flows. Figure 6 is a diagram of said system:

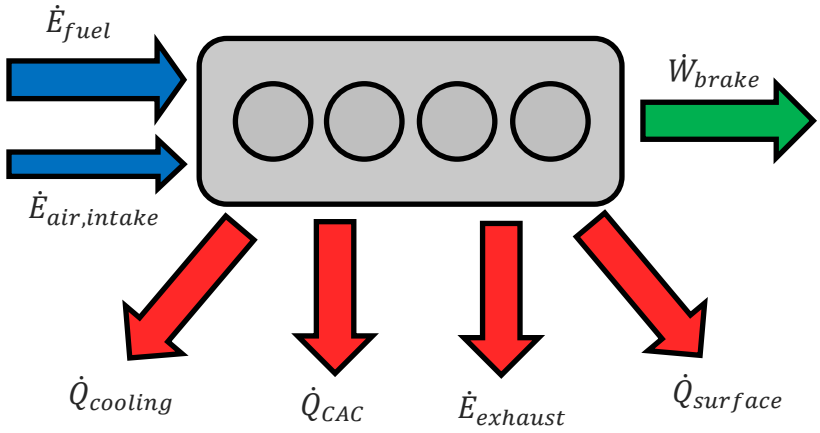

Figure 6. Diagram of engine depicting various mass and energy fluxes

Assuming steady state operation, the application of the first law of thermodynamics on a rate basis results in the following,

$$\dot{E}_{fuel} + \dot{E}_{air,intake} - \dot{E}_{exh} = \dot{W}_{brake} - \dot{Q}_{cool} - \dot{Q}_{CAC} - \dot{Q}_{surf} \quad (12)$$

where Table 7 defines the above terms.

Table 7. Definition of engine energy balance terms

Term	Definition
$\dot{E}_{fuel}$	Energy input via fuel
$\dot{E}_{air,intake}$	Energy input via air
$\dot{E}_{exh}$	Energy output via exhaust
$\dot{W}_{brake}$	Useful work by engine
$\dot{Q}_{cool}$	Heat rejected by coolant
$\dot{Q}_{CAC}$	Heat rejected by charge air cooler
$\dot{Q}_{surf}$	Heat rejected by engine surface

Each of these terms is calculated using measurements from the engine in conjunction with known tabulations or correlations. The subsequent sections detail the specifics of each of these calculations.

3.5.4. Fuel Energy

The total energy supplied to the engine via the fuel is estimated using the following,

$$\dot{E}_{fuel} = \dot{m}_{fuel}\, Q_{LHV} \tag{13}$$

where $\dot{m}_{fuel}$ is the mass flow rate of the fuel and Q_{LHV} is the lower heating value of the fuel.

The heating value of a fuel equals the total amount of energy extracted from its combustion starting from an initial temperature of 25 °C (298 K). There are two heating values typically specified for any fuel- a gross (or "higher") and a net (or "lower") value. The higher heating value assumes that all of the resulting water vapor is condensed into a liquid state after combustion, thereby releasing its latent heat of vaporization. In contrast, the lower heating value assumes that the water remains in its vapor state after combustion. The lower heating value is used in this study because the water exiting the engine remains in its vapor state due to the high exhaust temperatures, making any extraction of energy from its condensation impossible.

During normal operation, some portion of the supplied fuel is not injected into the engine and recirculates through the fuel tank. The mass flow rate of this unused fuel is properly accounted through the placement of the flow meter and overall design of the fuel supply system. Consequently, its chemical energy is accounted for; however, some thermal energy is accumulated as passes through the engine. Before reentering the fuel pump, the fuel is cooled back to ambient temperature by a heat exchanger to ensure a constant temperature fuel supply. While the heat rejected by this process is nonzero, it is assumed to be small relative to the other energy fluxes and is therefore neglected.

3.5.5. Intake Air Energy

Like the fuel, the intake air carries energy with it into the engine that must be accounted for in the balance,

$$\dot{E}_{air,intake} = \dot{m}_{air}\, h_{air} \tag{14}$$

where $\dot{m}_{air}$ is the mass air flow rate through the LFE and h_{air} is the enthalpy of the air.

Since air is a known mixture of numerous gases with disparate properties, the corresponding mixture enthalpy on a per mass basis must be calculated from the following,

$$h_{mix} = \frac{1}{MW_{mix}} \sum_{i=1}^{mix} X_i\, \bar{h}_i \tag{15}$$

where X_i is the mole fraction of a constitutive gas, $\bar{h}_i$ is its corresponding molar enthalpy, and MW_{mix} is the mixture's average molecular weight calculated using Eqn. (9).

For the most accurate estimation of the constitutive enthalpies, the NASA Glenn polynomials of the following form are used,

$$\bar{h}_i^0(T) = R\,T\,\left[a_1 + \frac{a_2 T}{2} + \frac{a_3 T^2}{3} + \frac{a_4 T^3}{4} + \frac{a_5 T^4}{5} + \frac{a_6}{T}\right] \tag{16}$$

where R is the universal gas constant, T is the temperature in Kelvin, and $a_1 - a_6$ are the least-squares fit constants specified by the NASA Glenn Research Center [42]. To

maintain a reference temperature consistent to that used for the fuel, all the gas enthalpies are referenced to 25 °C (298 K) by using the following,

$$\bar{h}_i(T) = \bar{h}_i^0(T) - \bar{h}_i^0(298) \tag{17}$$

where $\bar{h}_i^0(298)$ is the gas' molar enthalpy at 298 K, a value which is tabulated for all gases [42].

3.5.6. Exhaust Energy

Similar to the intake air, the exhaust gases carry energy out of the engine,

$$\dot{E}_{exh} = \dot{m}_{exh}\, h_{exh} \tag{18}$$

where $\dot{m}_{exh}$ is the mass flow rate of the exhaust and h_{exh} is the enthalpy of the exhaust gas mixture. The enthalpy of the exhaust mixture is calculated from the measured exhaust composition using a procedure similar to Section 3.5.5.

However, to properly account for the energy still available in the exhaust, the heat of combustion must be added for species which have not been fully oxidized, i.e. CO and HC emissions. For these cases, Eqn. (17) becomes the following:

$$\bar{h}_i(T) = \bar{h}_i^0(T) - \bar{h}_i^0(298) + \Delta\bar{h}_{c,i}^0 \tag{19}$$

where $\Delta\bar{h}_{c,i}^0$ is the heat of combustion of the species. This addition of an energy term creates a relationship between exhaust energy and CO and HC emissions, which is further discussed in Section 4.2.6.

Assuming steady state conditions with no mass accumulation in the system, the mass of the exhaust gases can be calculated through the application of mass conservation,

$$\dot{m}_{exh} = \dot{m}_{fuel} + \dot{m}_{air} \tag{20}$$

3.5.7. Brake Power

The useful energy output from the engine in the form of torque through a driveshaft can be calculated directly from the measured dyno torque and rotational speed,

$$\dot{W}_{brake} = 2\pi\, T_{dyn}\omega_e \tag{21}$$

where T_{dyn} is the applied torque and ω_e is the rotational speed of the engine and dyno.

3.5.8. Coolant Heat Transfer

As the coolant passes through the engine's air-liquid heat exchanger, commonly known as the "radiator," thermal energy is transferred from the coolant to the ambient air. This transfer naturally results in a corresponding temperature drop across the radiator. Assuming that the coolant has not boiled prior to entering the radiator, the total amount of heat transfer to the surroundings is dictated by Eqn. (22)

$$\dot{Q}_{cool} = \dot{m}_c\, C_c\left(T_{c,i} - T_{c,o}\right) \tag{22}$$

where $\dot{m}_c$ is the mass flowrate of the coolant, C_c is the mass specific heat of the coolant, and $T_{c,i}$ and $T_{c,o}$ are the inlet and outlet coolant temperatures, respectively.

The mass flow rate of the coolant is calculated from the frequency of the turbine flow meter's output signal using Eqn. (23),

$$\dot{m}_c = \rho_c \frac{f}{k_t} \tag{23}$$

where f is the frequency of the turbine's signal, k_t is a calibrated constant for the turbine relating frequency to volumetric flow rate, and ρ_c is the density of the coolant.

By using tabulated experimental values of density and specific heats for mixtures of water and ethylene-glycol [34], the steady state heat transfer by the radiator can be calculated. For the sake of simplicity, the density and specific heat are evaluated at the average temperature between the inlet and outlet. Since the temperature change through the radiator is typically less than 5 °C, the properties of the coolant do not differ significantly from the average, making this a valid approximation.

3.5.9. Charge Air Heat Transfer

Assuming steady state with minimal pressure change, an application of the first law of thermodynamics to the charge air cooler (CAC) results in the following relationship:

$$\dot{Q}_{CAC} = \dot{m}_{CAC}\,(h_{in} - h_{out}) \tag{24}$$

where $\dot{m}_{CAC}$ is the mass flow rate of fresh air, and h_{in} and h_{out} are the enthalpies of the air mixture at the inlet and outlet. Since the CAC for this test engine is located upstream of the inlet of EGR into the intake pipe, the EGR is not cooled by it and is not included in this calculation. The enthalpies are calculated using the same procedure as Section 3.5.5.

3.5.10. Surface Heat Transfer

The heat transfer from the surface of the engine is assumed to consist of both convective and radiative components which act in parallel to remove energy from the system:

$$\dot{Q}_{surf} = \dot{Q}_{conv} + \dot{Q}_{rad} \tag{25}$$

For the sake of simplicity, the engine is divided into ten regions which are approximated as flat plates and cylinders. The mean surface temperatures are estimated from a thermal imaging camera and its associated software as described in Section 3.3.3. The radiative heat transfer is calculated using the Stefan Boltzmann equation [33],

$$\dot{Q}_{rad} = \frac{\sigma}{\frac{1}{\varepsilon_{surf}} + \frac{1}{\varepsilon_{surr}} - 1}\, A_{surf}\, \left[\left(T_{surf}\right)^4 - \left(T_{surr}\right)^4\right] \tag{26}$$

where σ is the Stefan Botlzmann constant, ε is the emissivity of the surface or surroundings, A_{surf} is the estimated surface area, and all temperatures are in Kelvin.

Due to the location of the radiator and associated fans within the test bed, there is minimal air flow around the engine itself, so free convection conditions are assumed for all surfaces. Therefore, the Rayleigh number is used to assess the nature of the convection,

$$Ra = \frac{g\,\beta\,\left(T_{surf} - T_{\infty}\right) L^3}{\nu\,\alpha} \tag{27}$$

where g is the acceleration due to gravity, β is the thermal expansion coefficient, ν is the kinematic viscosity, α is the thermal diffusivity, T_∞ is the temperature of the fluid far from the surface, and L is the characteristic length of the surface.

All properties of the fluid (β, ν, α) are evaluated at the film temperature,

$$T_{film} = \frac{T_{surf} + T_\infty}{2} \tag{28}$$

In addition, the characteristic length depends on the shape and physical orientation of the surface, shown in Table 8.

Table 8. Characteristic length for each surface

Surface Type	**Definition**
Vertical Plate	$Height$
Horizontal Plate	$\frac{Area}{Perimeter}$
Horizontal cylinder	$Diameter$

With the Rayleigh number determined for each surface, various empirical correlations are used to calculate the Nusselt number (*Nu*); the choice of which depends on the surface type and the nature of the convection, namely laminar or turbulent [33]. From the Nusselt number, the average convective heat transfer coefficient can be calculated,

$$\bar{h}_{conv} = \frac{k\, Nu}{L} \tag{29}$$

where k is the thermal conductivity of the fluid evaluated at the film temperature. Finally, the steady state convective heat transfer rate can be calculated using Newton's law of cooling [33],

$$\dot{Q}_{conv} = \bar{h}_{conv}\, A_{surf} \left(T_{surf} - T_\infty\right) \tag{30}$$

3.5.11. Remainder of Energy

Any remainder of the input energy that is unaccounted for by the calculations in Sections 3.5.4-3.5.10 is estimated by the following,

$$\dot{E}_{remainder} = \dot{E}_{fuel} + \dot{E}_{air,intake} - \dot{E}_{exh} - \dot{W}_{brake} - \dot{Q}_{cool} - \dot{Q}_{CAC} - \dot{Q}_{surf} \quad (31)$$

This term serves as a "check-sum" which ensures that the majority of the input energy is captured by all the calculated energy terms.

3.5.12. Energy Balance Uncertainty

Most of the error calculations in this study are based on the day-to-day variation in the data since this overshadows any uncertainty caused by measurement bias or random error. However, the uncertainty in the energy balance resulting from these bias and random fluctuations is calculated in order to quantify the error inherent to the energy balance. Kline-McClintock and other standard techniques at a 95% confidence level are used to perform this analysis [35]. The uncertainty for each component of the energy balance is summed to produce an aggregated term which serves as a basis of comparison for the remainder energy of Section 3.5.11. If the total uncertainty is equal or greater than the residual energy, then the majority of this "check-sum" is most likely due to the propagation of error from the physical measurements.

3.5.13. Brake Specific NO_X Emissions

Typically, NO_X emissions standards are specified in terms of mass per mile or power. For the purpose of this study, the concentrations of NO_X in the exhaust are converted to a brake specific equivalent ($BSNO_X$) through the following,

$$BSNO_X = \dot{m}_{exh} \frac{Y_{NO_X}}{\dot{W}_{brake}} \left(\frac{MW_{NO_X}}{MW_{exh}} \right) \quad (32)$$

Although NO_X is actually a mixture of various oxides of nitrogen, these emissions are typically expressed in terms of NO_2 equivalents [43], so the molecular weight of NO_2 is used for this calculation.

3.5.14. Efficiencies

Since literature tends to be inconsistent in defining efficiencies for internal combustion engines, the efficiency metrics used in this study are specified in this section for clarity, using Heywood as a basis [6].

The combustion efficiency (η_c) indicates the degree to which the fuel's chemical energy has been released during the combustion process.

$$\eta_c = \frac{released\ fuel\ energy}{fuel\ energy\ input} = \frac{\dot{m}[h_R(T_A) - h_P(T_A)]}{\dot{m}_{fuel}\, Q_{LHV}} \tag{33}$$

where $\dot{m}$ is the mass flow rate of fluids through the engine, and h_R and h_P indicate the average mass specific enthalpies of the reactants and products respectively. In practice, this efficiency can also be calculated from the exhaust concentrations of incomplete combustion products, i.e. CO and HC.

All of this released energy is not converted into useful work, so it is helpful to define a thermal conversion efficiency (η_t) relating the two,

$$\eta_t = \frac{net\ work\ output}{released\ fuel\ energy} = \frac{\dot{W}}{\eta_c \dot{m}_{fuel}\, Q_{LHV}} \tag{34}$$

where $\dot{W}$ is the measured rate of work of the engine, either indicated or brake.

Lastly, the fuel conversion efficiency (η_f) serves as a metric of the overall efficiency of the engine, relating the useful work output to the input fuel energy.

$$\eta_f = \frac{net\ work\ output}{input\ fuel\ energy} = \frac{\dot{W}}{\dot{m}_{fuel}\, Q_{LHV}} = \eta_t \eta_c \tag{35}$$

Fuel conversion efficiency is often referred to as thermal efficiency in literature; therefore, any references to thermal efficiencies reported by previous studies are actually fuel conversion efficiencies in the terminology of this study. Lastly, in this study, all efficiencies are defined in "brake" terms using the brake power calculated from the measured torque and speed of the dynamometer.

3.6. Parameter Summary

Since there are numerous parameters plotted and discussed in the following sections, Table 9 is included as a reference guide to quickly locate the measurement or calculation specifics of each variable.

Table 9. Measurement and calculation methods summary

Parameter	Calculated or Measured	Method
EGR Level	Calculated	See Section 3.5.1
Injection Timing	Measured	Set by controller
Exhaust concentrations of NO_X, CO, CO_2, and HC	Measured	See Section 3.3.4
Filter Smoke Number	Measured	See Section 3.3.4
Brake Specific NO_X emissions	Calculated	See Section 3.5.13
Cylinder Pressure	Measured	See Section 3.3.2
Apparent heat release rate	Calculated	See Section 3.5.2
Combustion efficiency	Calculated	See Section 3.5.14
Thermal conversion efficiency	Calculated	See Section 3.5.14
Fuel conversion efficiency	Calculated	See Section 3.5.14
Engine energy fluxes	Calculated	See Sections 3.5.3 — 3.5.10

4. RESULTS AND DISCUSSION

4.1. LTC Characterization

4.1.1. Objective

As previously discussed, the objective of the first portion of this study is the attainment of LTC operation with the light-duty diesel test engine. In the following sections, the criteria for this realization will be defined, and the behavior of other parameters of interest will be explored to further validate LTC operation.

4.1.2. NO_x and PM Emissions

Since there are numerous means to achieve LTC conditions, there are, of course, numerous differing criteria for defining the achievement of LTC operation. From an extensive literature review, the criteria which appears to be generally and broadly accepted is a 90% reduction in $BSNO_X$ emissions while maintaining an equivalent PM concentration [44]. These criteria will be used as a basis for identifying LTC conditions for this study. For the analysis, the conventional timing of 8 °bTDC and 0% EGR is chosen as the baseline with which the NO_X and PM emissions of the other testing conditions are compared.

The exhaust concentrations of NO_X and filter smoke number from the EGR and injection timing sweeps are shown in Figure 7.

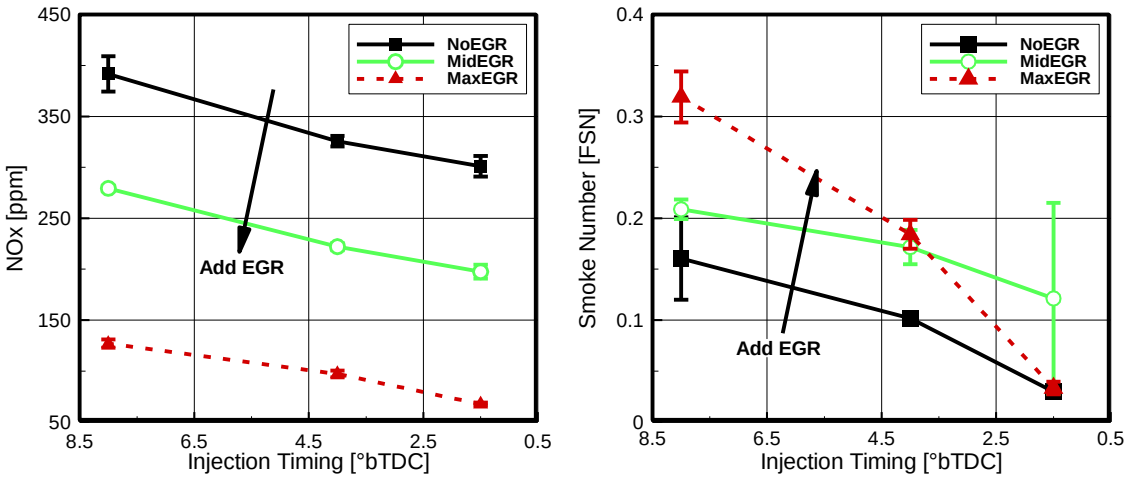

Figure 7. Exhaust concentrations of NO_X (left) and filter smoke number (right) as a function of injection timing and EGR level

In general, the "NO_X-soot tradeoff" of conventional combustion holds true with increased EGR levels resulting in higher soot and lower NO_X emissions. One point, namely the 1.5 °bTDC timing and 35% EGR point, defeats this tradeoff. This test condition resulted in a smoke number similar to the 0% EGR level at the same injection timing while significantly reducing NO_X. Figure 8 shows the same data in an alternative manner for better identification of this trend.

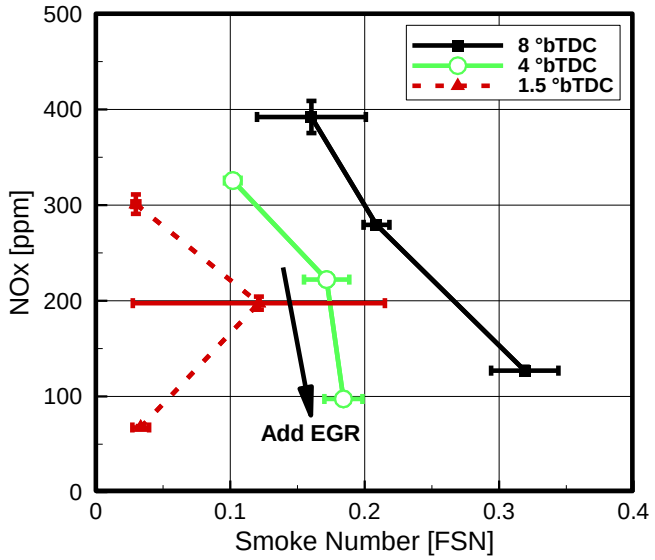

Figure 8. NOx concentration as a function of smoke number for three injection timings and three EGR levels.

In this figure, the "conventional timing" of 8 °bTDC clearly demonstrates a trade-off between the two emissions, with one decreasing at the cost of the other increasing. Similarly, the mid timing of 4 °bTDC shows the same behavior, but the smoke number for the highest level of EGR is not as dramatically increased. Finally, at a late timing of 1.5 °bTDC, the trend reverses for the highest EGR level and both pollutant concentrations reach low levels.

It is important to note that the large error bar associated with the mid-EGR, 1.5 °bTDC data point is due to a high smoke number measured on the second day of testing, as seen in Figure 9.

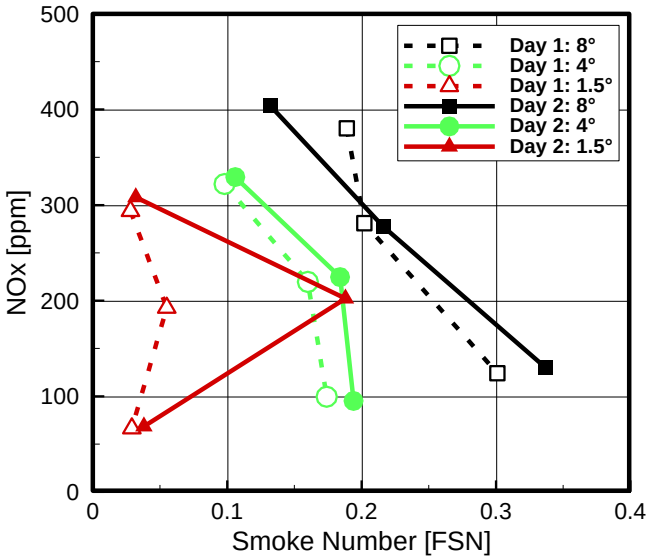

Figure 9. NOx concentration as a function of smoke number for both days of data

This particular point was the last test point taken on that day, and its anomalous nature was not noticed until post-testing data processing began. However, its larger value can most likely be attributed to equipment malfunction rather than a true change in behavior. Upon resumption of testing for the second phase of this study, namely the LHR-LTC operation, several equipment issues surfaced with the smoke meter, any one of which could have contributed to the larger value measured on the second day.

The data displayed in Figure 9 is also useful in displaying the sensitivity of the smoke meter used to measure the soot emissions. In past studies [38], some concerns have been raised as to how sensitive this device is at the lower end of its measuring range. The slightly different values between datasets indicate that even at low smoke numbers, the smoke meter remains sensitive enough to measure day-to-day variation.

However, while the reduction in NO_X emissions is significant, it does not appear to represent a 90% reduction as specified previously as the criteria for identifying LTC operation. Specifically, there is approximately an 82% reduction between the baseline conditions and the lowest value at 1.5° bTDC and 35% EGR. This apparent discrepancy occurs because the concentration values shown in Figure 8 represent a volumetric

fraction of the total exhaust and do not include any changes of exhaust flow rates or brake power.

After converting these measurements to their equivalent brake specific values, the reduction is more pronounced as displayed in Figure 10.

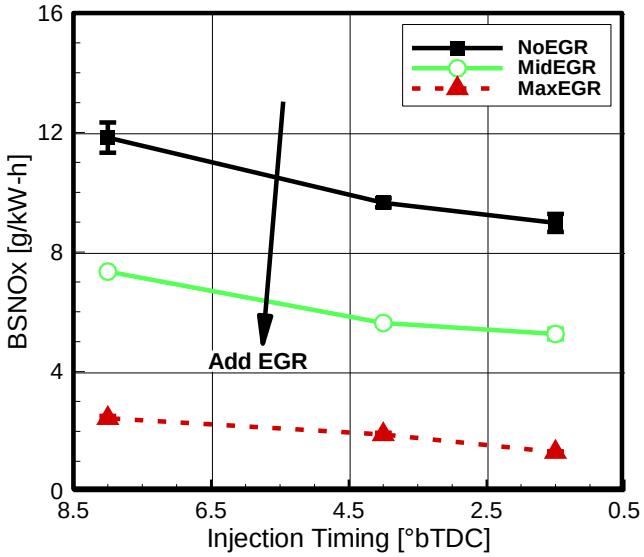

Figure 10. Brake specific NO_X emissions as a function of injection timing and EGR level

Putting this information in terms of reduction in $BSNO_X$ relative to the 0% EGR test points makes an easier identification of which points meet the 90% criterion, as seen in Figure 11.

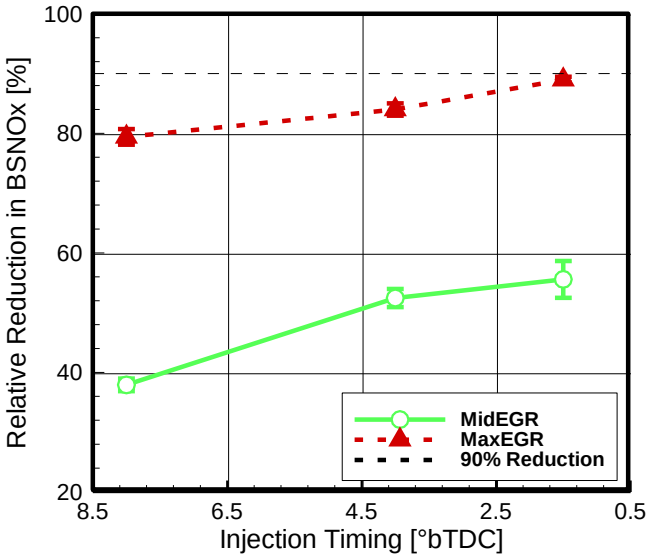

Figure 11. Relative reduction in $BSNO_X$ as a function of injection timing and EGR level

When described in this manner, the average NO_X emissions are reduced by approximately 89% at the 1.5°bTDC and 35% EGR testing condition compared to the baseline. This reduction technically falls short of meeting the criteria; however, considering the day-to-day variation, particularly in the baseline measurement at 8 °bTDC and 0% EGR, it is reasonable to suppose that a 90% reduction has been achieved. This combined with a simultaneous reduction in smoke number confirms that LTC operation has been realized on the test engine with an injection timing of 1.5°bTDC and 35% EGR.

4.1.3. Supplementary Trends

As previously discussed, LTC conditions have other effects on engine operation and performance, some of which are undesirable. By increasing the amount of EGR and retarding the injection timing, the characteristics of the combustion process within the engine's cycle are altered significantly. To illustrate this alteration, the in-cylinder pressure profiles and AHRRs for selected testing conditions are shown in Figure 12.

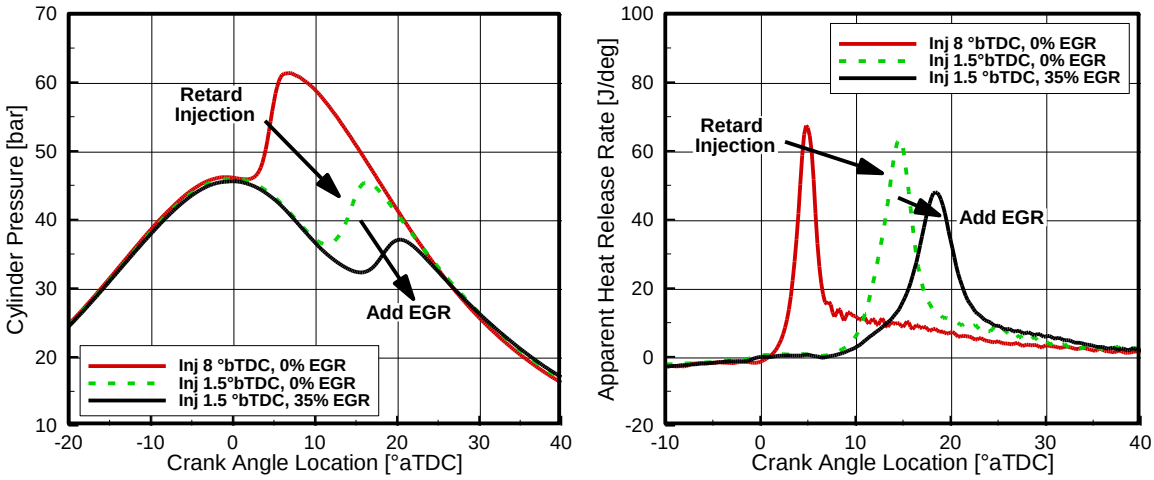

Figure 12. In-cylinder pressure (left) and AHRR (right) as a function of engine operation

Clearly at retarded timings, the spikes in pressure and AHRR caused by the fuel's combustion are moved further into the expansion stroke of the cylinder. While this modification to the combustion process is what results in the lower peak pressures and temperatures that reduce NO_X production, it also serves to push combustion further into the expansion stroke of the piston where the lower mixture temperatures can prevent the fuel from completely combusting. To further exacerbate the issue, the addition of EGR reduces the intensity of combustion which necessitates an increase in combustion duration in order to fully consume the fuel in the cylinder. To say this in another way, the energy released by the fuel is represented by the area under the AHRR curve, so the lower AHRRs must be spread across more of the cycle to release the same energy. A longer duration is particularly evident in the widening of the AHRR spike at an injection timing of 1.5 °bTDC and 35% EGR. This increase in duration in turn pushes the tail end of the combustion process even further into expansion stroke, resulting in more incomplete combustion. This incomplete combustion is most evident in the increased exhaust concentrations of CO and HC, as shown in Figure 13.

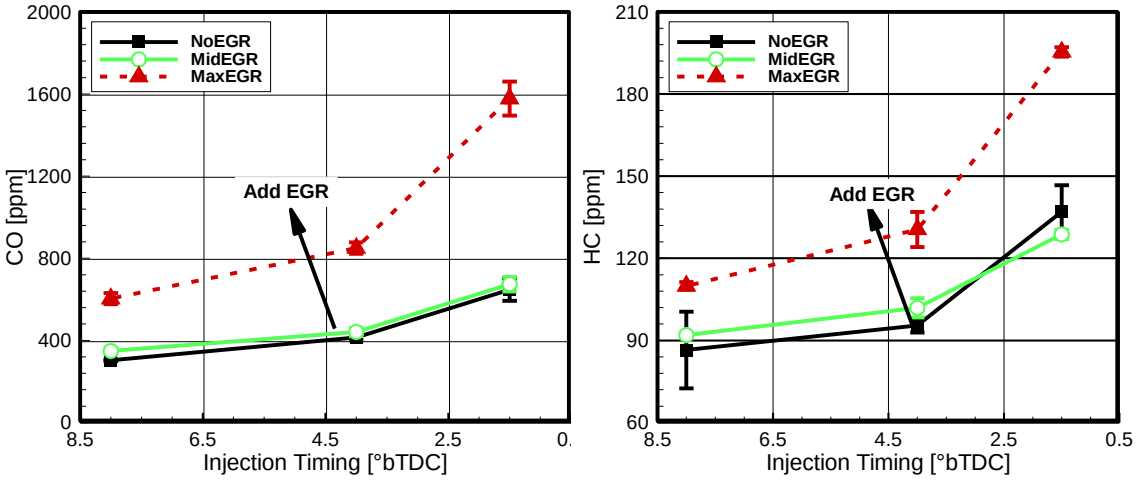

Figure 13. Exhaust concentrations of CO (left) and HC (right) as a function of injection timing and EGR level

The concentrations for both pollutants increase with retarded timings and increased EGR levels, with dramatically increased values at the LTC testing condition, reaching approximately 420% and 125% of the baseline CO and HC concentrations, respectively. While increases in these pollutants can be dealt with using exhaust treatment techniques, they serve as indicators of a decrease in combustion efficiency, as shown in Figure 14.

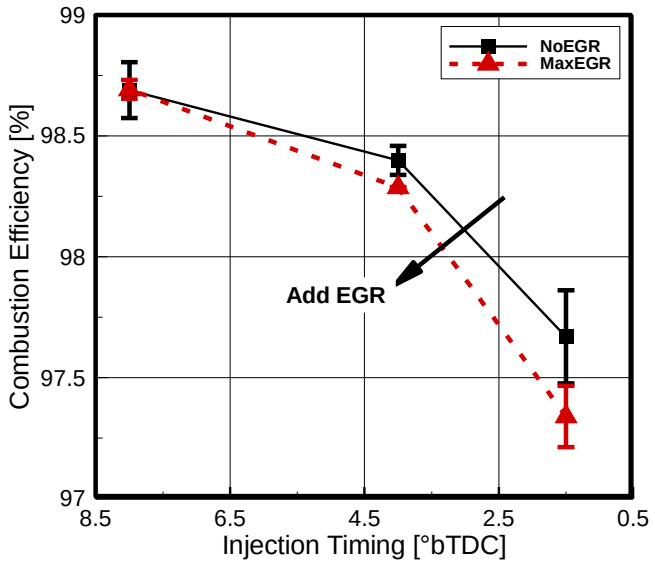

Figure 14. Combustion efficiency as a function of injection timing and EGR level

Clearly with additional EGR and later injection timings, the fuel is not as fully combusted. In addition, by moving the combustion process farther into the expansion stroke, the effective expansion ratio of the piston is reduced. Consequently, less useful work can be extracted from the mixture by the piston, and the brake fuel conversion efficiency decreases accordingly as depicted in Figure 15.

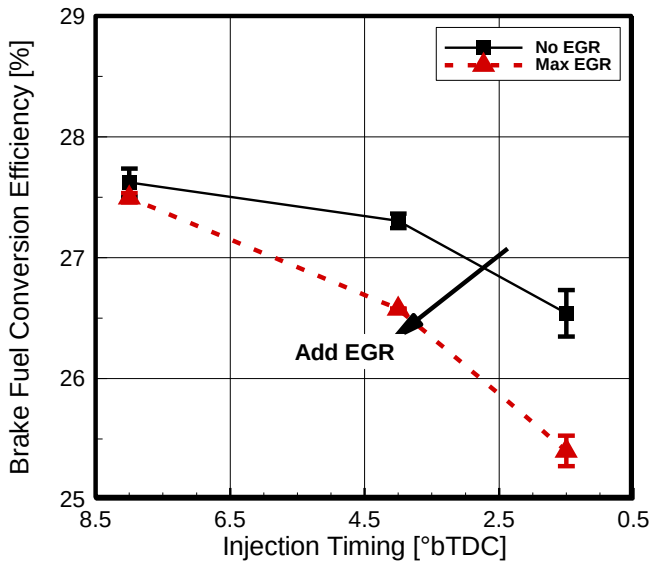

Figure 15. Brake fuel conversion efficiency as a function of injection timing and EGR level

It is important to note that the compounding effects of incomplete combustion and diminished expansion ratio both cause the fuel conversion efficiency of the engine to degrade significantly from the baseline conditions of 8 °bTDC and 0% EGR. At the LTC point, this represents a 2.2% decrease in absolute efficiency and an 8% decrease relative to the baseline, which represents a substantial loss in efficiency.

4.1.4. Discussion

The results demonstrate that LTC operation is possible on this test engine, resulting in the desired decrease in NO_X and soot emissions. In addition, the trends of increased CO and HC emissions as well as a decreased efficiency match well documented side effects of LTC (see Section 2.1 for specifics), further corroborating the assertion that LTC conditions have been realized.

There is some question as to whether these reductions in NO_X and soot are due to a new combustion regime or just a result of the reduction in the energy released from the fuel. Since combustion efficiency does not significantly drop between the "conventional" and LTC test points, it would appear that the energy released remains

relatively constant and that a new combustion regime has been realized. However, an exhaustive discussion of the possible root causes of LTC behavior falls beyond the scope of this study, and would be best served by a more in-depth exploration in a future study.

With an understanding of the engine control parameters, namely injection timing and EGR rate, that will produce LTC conditions, LHR techniques can be applied to both the "conventional" and LTC test points to explore how the undesirable consequences of incomplete combustion and efficiency losses can be mitigated.

4.2. LHR-LTC Operation

4.2.1. Objective

The objective of the second portion of this study is to quantify the degree to which the adverse effects of LTC can be mitigated by elevated coolant temperatures while still maintaining the desired reduction in NO_X and PM emissions. Specifically, the 90% reduction in $BSNO_X$ and maintenance of PM emissions previously used to identify LTC should be retained. As for the undesirable effects, the CO and HC emissions, combustion efficiency, and brake fuel conversion efficiency will be studied in order to establish trends in their improvement. In addition, the total improvement or degradation from the typical operating ECT of 90 °C will also be quantified.

4.2.2. NO_X and PM Emissions

To ensure that the engine is still operating at LTC conditions for all coolant temperatures, the NO_X and PM emissions in the exhaust must be examined in detail. Figure 16 depicts the NO_X emissions as a function of ECT for both combustion regimes.

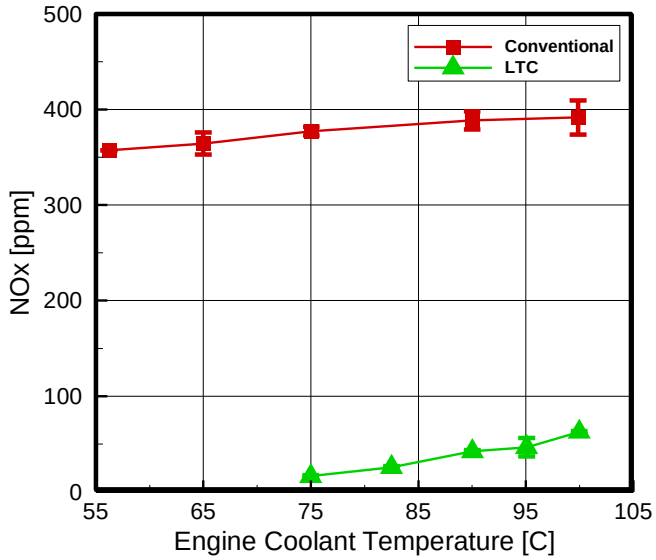

Figure 16. Exhaust concentrations of NO_X as a function of ECT

As apparent from Figure 16, the concentration of NO_X in the exhaust for both conventional and LTC increases as a function of ECT. This is likely due to higher in-cylinder temperatures from the reduced heat transfer from the cylinder into the engine block which should in turn produce more NO_X. The LTC emissions appear to be more sensitive to this effect, as shown in Table 10. For the sake of comparison, the minimum coolant temperature for the conventional condition is chosen to be the same as the LTC conditions.

Table 10.Comparison of maximum and minimum NO_X values

Testing Condition	**Min. Value**	**Max. Value**	**Absolute Difference**	**Relative Difference**
Conventional	377 ppm @ 75°C	391 ppm @ 100°C	14 ppm	3.7%
LTC	16.3 ppm @ 75°C	62.6 ppm @ 100°C	46 ppm	284%

This difference in sensitivity to coolant temperature is likely due to the lower gas mixture temperatures present within LTC. These lower temperatures result in a smaller temperature gradient between the mixture and the wall, which is more sensitive to small changes in either end of the gradient since these represent a larger portion of the total temperature difference. Therefore, a change in the wall temperature due to higher or lower coolant temperature will have a more significant effect at LTC conditions on the temperature gradient and consequently the heat transfer rate and corresponding in-cylinder temperature. This in turn has an amplified influence on NO_X production due to the highly temperature sensitive nature of its production mechanisms (refer to Section 1.2.1).

It is important to note that the error bars for the 56.5°C conventional combustion test point are zero in Figure 16 and all subsequent plots. This test point was unachievable on the second test day due to higher ambient temperatures. Consequently, there was no data from which to perform statistical analysis, and all error bars are correspondingly zero.

To assess if the test points still meet the established 90% criteria, the emissions must be converted to their equivalent $BSNO_X$ values, shown in Figure 17.

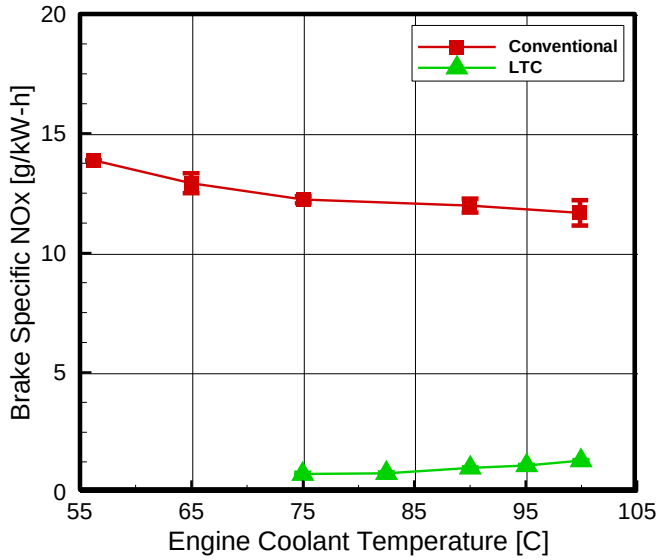

Figure 17. Brake specific NO_X emissions as a function of ECT

Interestingly, this conversion reverses the trend of the conventional combustion conditions due to the higher values of brake power produced at the higher coolant temperatures. Additionally, while the LTC trend still increases as a function of temperature, its slope is flattened by the increase in brake power. To better identify if the criteria are met, the reduction in $BSNO_X$ relative to conventional combustion is calculated for the LTC testing conditions, as shown in Figure 18. As a side note, since no data existed for conventional combustion at ECTs of 82.5 °C and 95°C, the relative reduction is calculated using a conventional BSNOx obtained from linear interpolation between the measured values.

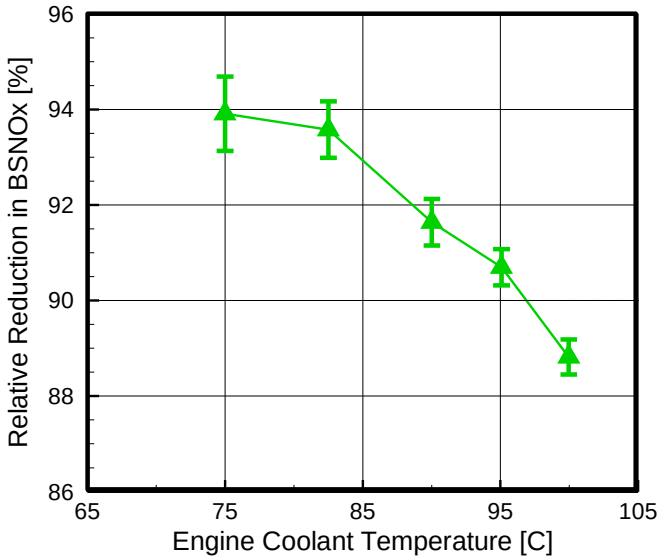

Figure 18. Relative reduction in $BSNO_X$ for LTC conditions as a function of ECT

As apparent from Figure 18, the relative reduction in $BSNO_X$ decreases in magnitude with elevated coolant temperatures, eventually dipping below the 90% criteria at a coolant temperature of 100°C. Obviously, while this means that the 100°C test point does not strictly meet the specified criteria, it is still approximately 89%, which represents a significant reduction in NO_X emissions.

To ensure that the PM emissions are at least maintained, filter smoke number is plotted as a function of ECT in Figure 19.

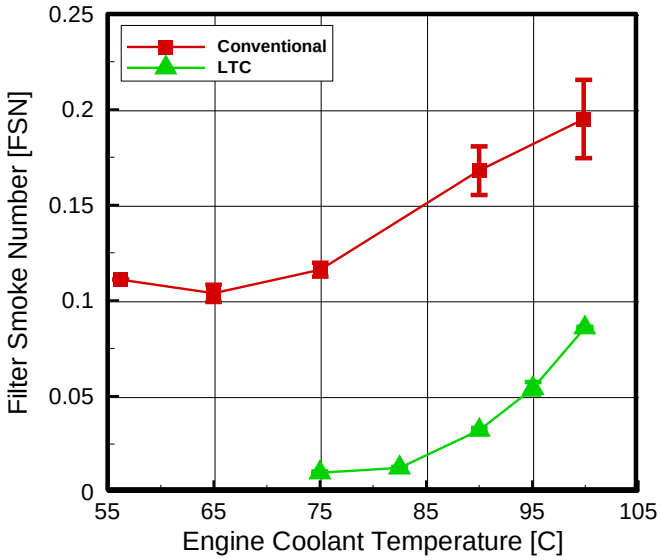

Figure 19. Filter smoke number as a function of ECT

The PM emissions for all LTC test points are lower than that of their corresponding conventional ECT test condition, thereby satisfying the second half of the LTC criteria. As for the trends, the PM emissions tend to increase as a function of ECT for both conventional and LTC conditions. This trend makes sense for LTC considering that increases in coolant temperature should result in higher mixture temperatures, pushing the net release of soot back up the "hump" into the conventional combustion region (refer to Section 1.2.2). However, the increase in PM emissions for conventional combustion runs counter to the expected "NO_X-soot" trade-off since NO_X emissions are also increasing with ECT. This behavior does correlate to a previous study that found an increase in soot production as a result of even a small increase in wall temperature [45]. In this current and the previous study, the elevated wall temperatures result in a decreased ignition delay (refer to Section 4.2.3) which causes reduced diffusion of air into the fuel spray. This leads to burning of the fuel in pockets with richer local equivalence ratios, thereby increasing soot production as a function of ECT.

4.2.3. Pressure and AHRR Trends

As established in Section 4.1.3, the in-cylinder combustion process can be altered significantly by changing engine control parameters, resulting in incomplete combustion and increased production of pollutants such CO and HC. To study the effect of ECT variation on combustion, the pressure and AHRR profiles are examined at the maximum and minimum values of ECT for conventional combustion. It should be noted that the cylinder wall temperature used in the calculation of the AHRR shown in Figure 20 was assumed to be constant across all the different ECTs studied. In reality, cylinder wall temperature should increase as a function of ECT; however, future work is needed to quantify this relationship. Due to this assumption, any discussion as to the behavior of AHRR as a function of ECT is qualitative in nature.

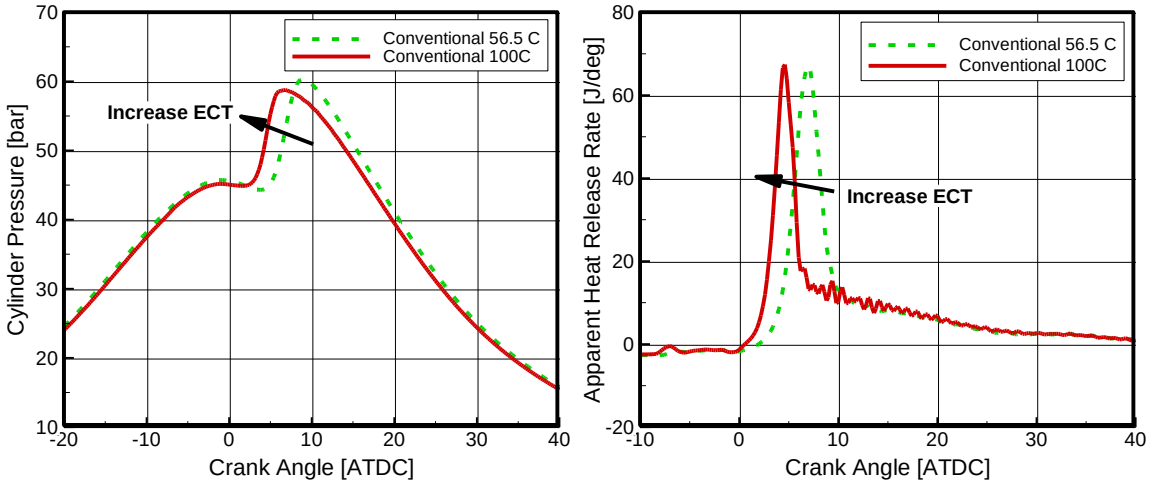

Figure 20. In-cylinder pressure (left) and AHRR (right) for conventional combustion as a function of ECT

The lower coolant temperature serves to push the combustion process further into the expansion stroke as well as slightly increase its duration. The decreased coolant temperature serves to increase heat transfer rates out of the cylinder, thereby cooling the gas mixture which results in longer ignition delays and combustion durations. These

shorter ignition delays at higher ECTs could be contributing to the expected increase in FSN as a function of ECT observed in Section 4.2.2 for conventional combustion. With the reduction in mixing time for the fuel and air, combustion would occur at richer equivalence ratios, resulting in greater soot production.

Aside from these small changes, the conventional combustion conditions are not significantly altered due to ECT variation, which in turn should not seriously affect HC and CO emissions or efficiency. In contrast, the combustion process of the LTC test points are substantially affected by ECT, as apparent from the pressure and AHRR profiles depicted in Figure 21.

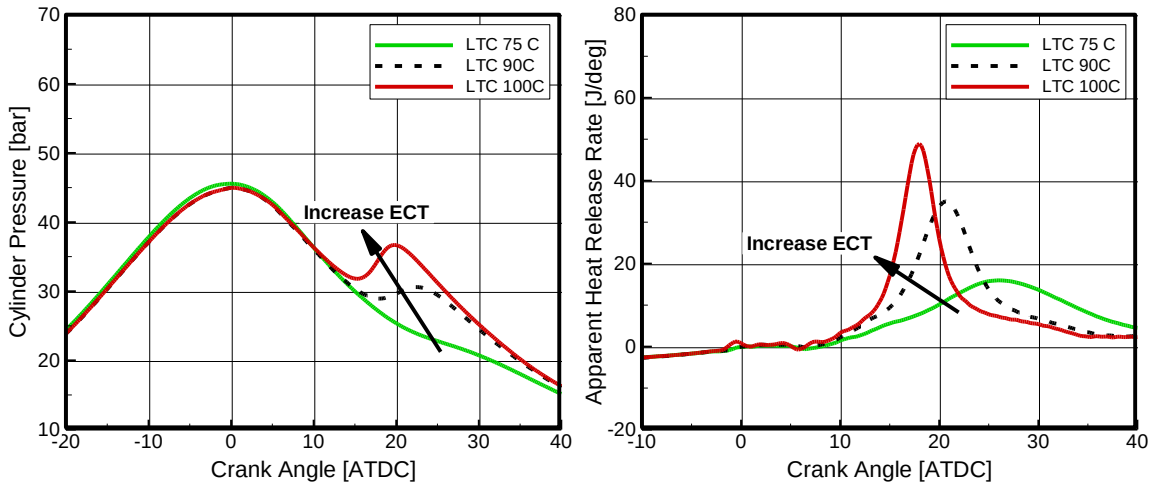

Figure 21. In-cylinder pressure (left) and AHRR (right) for LTC as a function of ECT

At the lowest coolant temperature, the cylinder pressure hardly deviates from that of a motoring pressure profile. Similarly, the spike in AHRR is half of the magnitude at 90°C and spread across a much larger range of the engine's expansion stroke. Both of these trends point to a combustion process in which the fuel is hardly burning at all due to in-cylinder pressures and temperatures which are too diminished to sustain combustion. As an interesting side note, if the ECT is decreased just a few degrees

below 75°C, the engine actually begins to misfire, starting with the cylinders closest to the inlet of coolant into the engine block from the radiator.

In contrast to this trend, when the ECT is increased to 100°C from its typical value of 90°C, both the pressure and AHRR profiles indicate a more robust combustion process. The in-cylinder pressure spike due to combustion is more pronounced and earlier in the engine cycle. Similarly, the peak AHRR is approximately 1.5 times the magnitude at 90°C, and the portion indicative of combustion is confined to a narrower portion of the expansion stroke. Again, these two trends point to a more complete combustion process at higher ECTs which should result in lower CO and HC emissions as well as higher combustion efficiencies. The following sections examine these parameters in more detail.

4.2.4. CO and HC Emissions

As previously discussed in Section 4.1.3, the exhaust concentrations of CO and HC, shown in Figure 22, serve as additional indicators of the completeness of combustion.

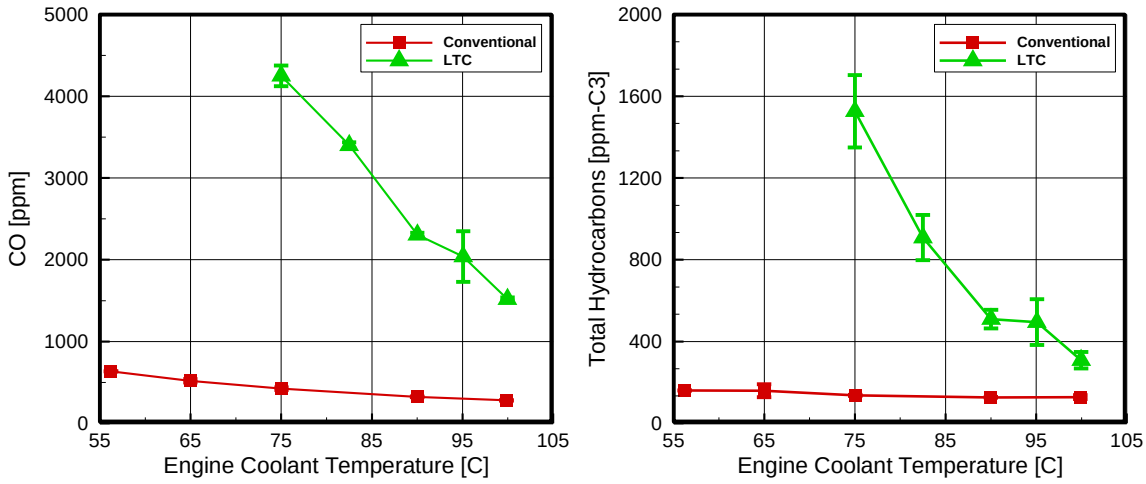

Figure 22. Exhaust concentrations of CO (left) and HC (right) as a function of ECT

Both CO and HC emissions decrease as a function of ECT, with the LTC conditions experiencing a more pronounced downward slope. In particular, the HC emissions are especially elevated at the lowest ECT values tested for LTC, reaching an order of magnitude larger than the conventional combustion at the 75°C test point. On the opposite end of the ECT range, both CO and HC emissions are decreased from the baseline conditions. While the values for LTC do not reach the same low levels as their conventional counterparts for the ECT range studied, the two trends appear to be converging on each other. If the coolant temperature is increased to even higher values, the HC and CO emissions will likely continue to converge, further reducing one of the drawbacks to LTC.

4.2.5. Efficiencies

Based on the exhaust species concentrations, the combustion efficiency is calculated for all test points and plotted in Figure 23.

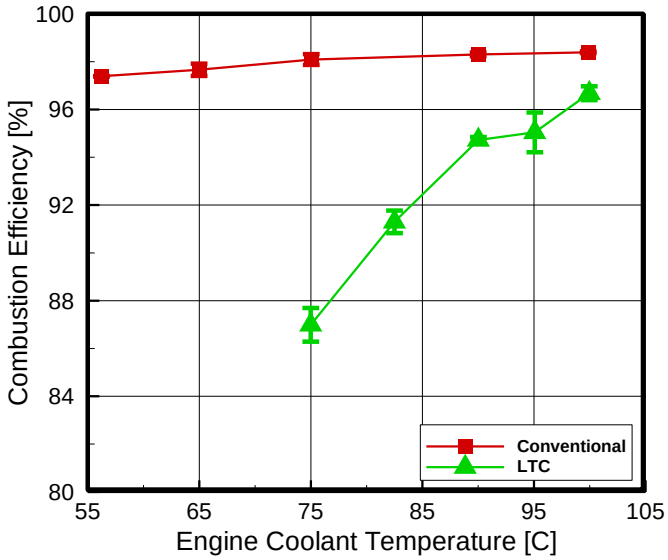

Figure 23. Combustion efficiency as a function of ECT

Unsurprisingly, combustion efficiency for both conventional combustion and LTC increase as a function of ECT, with the LTC trend exhibiting a steeper slope. Again, while the LTC values are still lower than their counterparts, they appear to be converging, and higher ECTs should lead to similar values for both conditions, assuming that the elevated temperatures do not lead to a shift in combustion behavior.

As an aside, the 95°C LTC point slightly deviates from the apparent trends in Figure 22 and Figure 23 and has a correspondingly larger error than its neighbors. This is likely due to an issue that was experienced with the common rail fuel pressure controller during the collection of this test point on the second day. Due to the malfunction, the rail pressure fluctuated wildly and the fuel was not injected at a consistent pressure, which would have resulted in large variations of combustion behavior and may have even led to impingement of the fuel spray on the cylinder wall prior to combustion. This would have contributed to the higher values of CO and HC (and correspondingly lower combustion efficiency) on the second day.

While combustion efficiency serves well as an indication of how well the fuel itself burns, the process of converting the released energy into useful work is where most of the inefficiencies lie. Friction losses, improper phasing of combustion, and heat transfer losses all contribute to the low thermal conversion efficiencies in Figure 24.

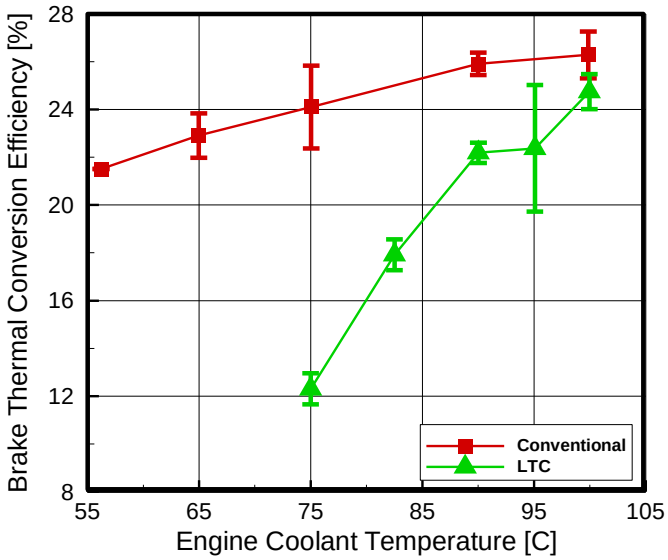

Figure 24. Brake thermal conversion efficiency as a function of ECT

The brake thermal conversion efficiency follows the same general behavior for both conventional and LTC conditions; however, the slopes of these trends appear steeper than with combustion efficiency, particularly with the conventional test points. There are several underlying reasons for this behavior. First, by phasing the combustion process further into the expansion stroke (refer to Section 4.2.3), the effective expansion ratio is reduced, and less work can be extracted from the gas mixture by the piston. In addition, a greater portion of the fuel's energy is being rejected through heat transfer into the coolant due to the larger temperature gradients at lower temperatures. Lastly, colder oil temperatures could lead to more viscous oil and therefore higher frictional losses.

Brake fuel conversion efficiency serves as an indicator of the overall engine efficiency, and displays an increasing trend as a function of ECT, as evident in Figure 25.

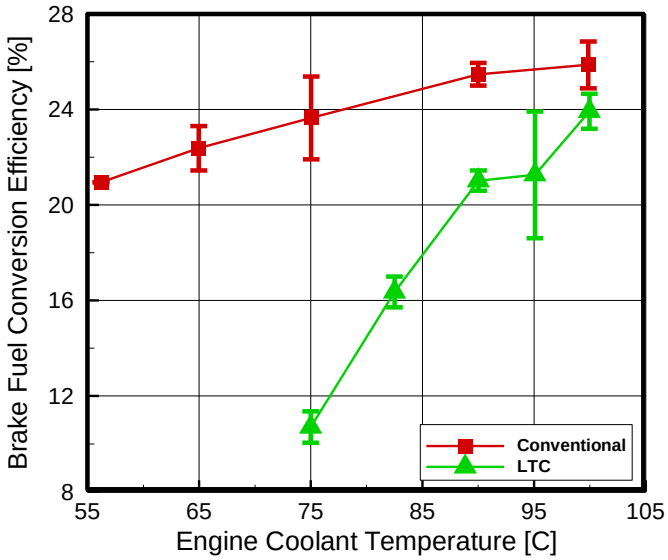

Figure 25. Brake fuel conversion efficiency as a function of ECT

Since it is the product of both combustion and thermal conversion efficiencies, the brake fuel conversion efficiency naturally displays a behavior similar the other two. Interestingly, the LTC efficiencies at high ECTs actually exceed those of conventional combustion at low ECTs, demonstrating just how strong an effect ECT has on the engine's overall efficiency. More importantly, there is a significant improvement in the brake fuel conversion efficiency for the LTC by increasing the ECT just 10°C from its baseline value. This amounts to an absolute increase of 2.9 percentage points (14% relative to the baseline conditions). In contrast, the conventional combustion only increases by 0.4 percentage points (1.5% relative to baseline) for the same increase in ECT. Consequently, the gap between the two conditions decreases from 4.4% at 90°C to 1.9% at 100°C. Therefore, while the efficiency lost by employing LTC techniques is not fully recovered, a more significant portion can be recouped at higher ECTs.

4.2.6. Energy Balance

To ensure the validity of these results, the energy balance discussed in Section 3.5.3 is applied to the engine for all the test points. The unaccounted or "check-sum" portion of the total energy that remains is depicted in Figure 26.

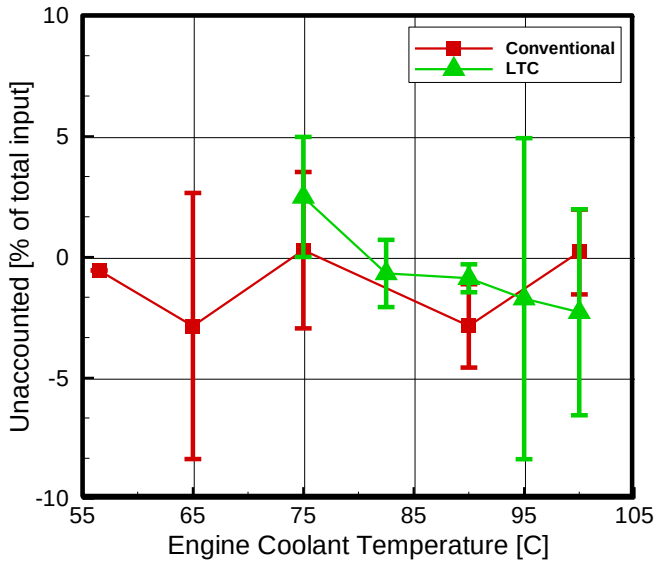

Figure 26. Unaccounted percentage of input energy as a function of ECT

Ideally, this quantities would be zero, indicating that all of the energy has properly accounted for by the calculations; however, a value within 3-5% of zero is not uncommon in previous studies [29, 30, 46]. This margin of error is adequate considering that there are the numerous terms that must be calculated from correlations and physical measurements, each of which contain error that propagates through the calculations. In most cases, the total uncertainty from all the terms is equal or greater in magnitude than the unaccounted energy (refer to Appendix A for uncertainty values). In addition, zero falls within almost all of the error bars in Figure 26, which are based on day-to-day variations, further emphasizing that the remainder energy is likely close to zero.

As for the actual results, the average residuals all fall within the expected 5% range. In fact, the test points of most interest, namely between 90°C and 100°C, fall close to zero; consequently, the assertions of improvements in efficiency and emissions of the LTC conditions are bolstered by these results.

It is important to note that a negative value of this remainder indicates that one or more of the calculated components is overestimated, resulting in more energy being consumed than is actually available from the fuel and air. This can point to inaccuracies in the actual calculations or that the engine may have not actually reached steady state conditions.

Since ECT is the independent variable for this study, a change in the rate of heat rejection to the coolant brings the engine to a new steady state condition, and its value is a strong indicator of whether the engine has actually reached steady state. Figure 27 shows the coolant heat rejection rate as a function of ECT for both conventional and LTC regimes.

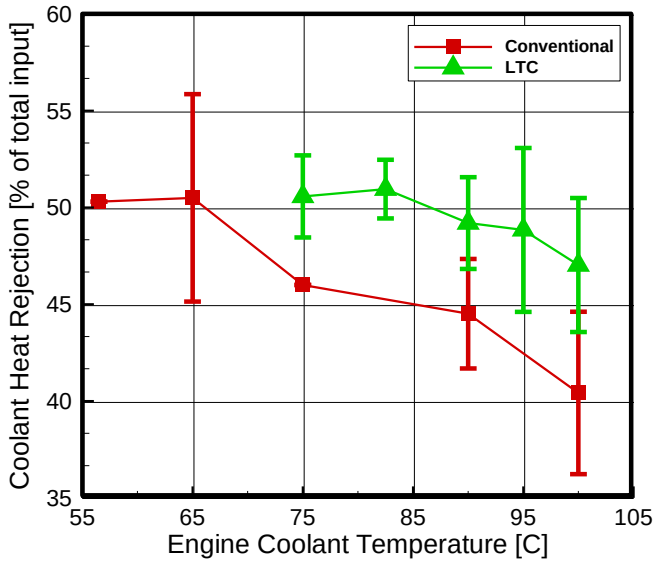

Figure 27. Percentage of input energy rejected through coolant as a function of ECT

A large error bar for a test point could indicate that the engine had not quite achieved a steady state on one day relative to the other. Upon deeper investigation into the raw data (refer to Appendix B for values), the coolant heat rejection rates on the second day were typically higher. These higher values can be explained in part by the higher ambient temperatures on the second day, which caused the heat transfer rate from the surface of the engine to be lower. Consequently, more energy had to be rejected to the coolant to maintain the same thermal state on the second day. However, the time allotted to reach steady state conditions may have not be sufficient for the second day, perhaps due to the second day's higher ambient temperatures which would have reduced the radiator's ability to reject heat to the environment. While coolant heat rejection rate was monitored during testing to confirm a constant value before data collection, more care must be taken in future tests to ensure that it has in fact reached its steady state value before data is collected. A future study of engine operation during the transition between test points would help establish a better understanding of its transient thermal behavior. This knowledge of transitory performance would also be useful in devising algorithms for controlling the engine's thermal state to actually achieve the indicated efficiency gains during LTC operation.

As for comparing the LTC and conventional test points, the heat rejection to the coolant is higher for all points of LTC. The bulk of this increase is due to the added heat load of the EGR cooler which is cooling down approximately the 35% EGR from its almost 200°C exhaust manifold temperature. This dumping of excess heat helps to increase the volumetric efficiency of the engine, but also results in more heat rejection to the coolant.

Other portions of the energy balance also point to some interesting trends. Next largest in its contribution to the energy balance is the brake power of the engine. As expected from the discussion in Section 4.2.5, the brake power increases as a function of ECT, as shown in Figure 28.

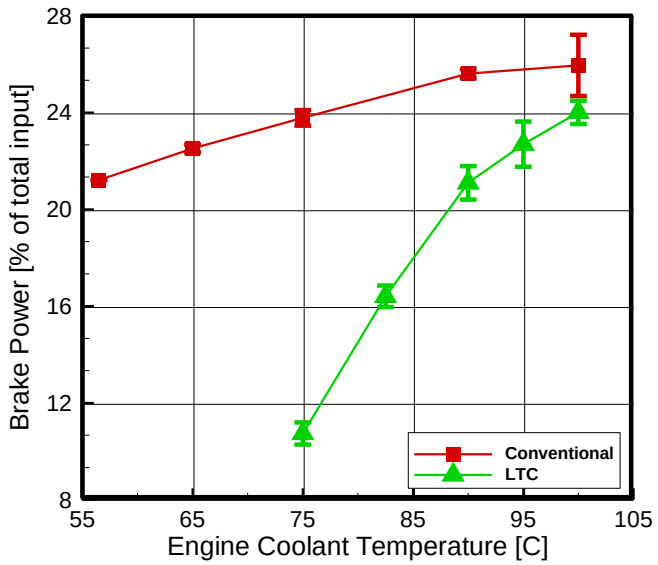

Figure 28. Percentage of input energy for brake work as a function of ECT

There is an important distinction to make when comparing these values to previous discussions of brake fuel conversion efficiency. While the brake fuel conversion efficiency only takes into account the energy of the fuel, the values in Figure 28 also include the enthalpy of the intake EGR/air mixture which causes them to differ slightly. Naturally, since the fuel's energy comprises the bulk of the input energy, this difference is minor, but it is important to note.

Falling close behind brake power in magnitude is the rate of energy lost to the exhaust, which Figure 29 depicts.

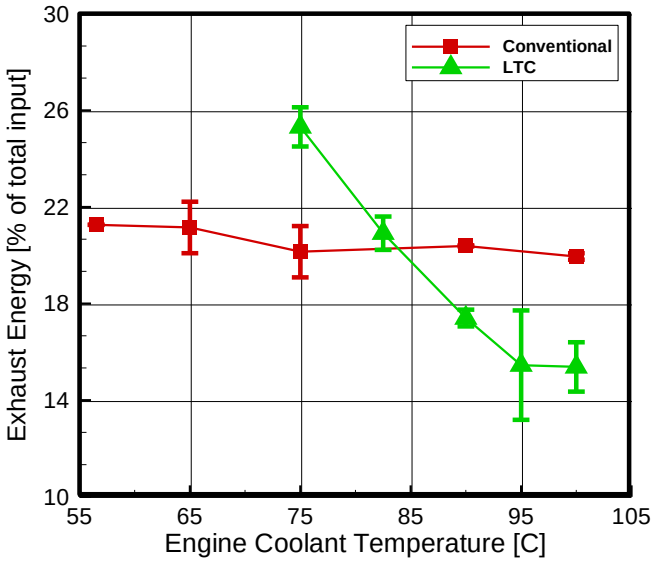

Figure 29. Percentage of input energy exiting in exhaust as a function of ECT

For the conventional test points, this value remains relatively constant around 21% because the flow rate and temperature of the exhaust does not significantly change throughout the ECT range studied, as shown in Figure 30.

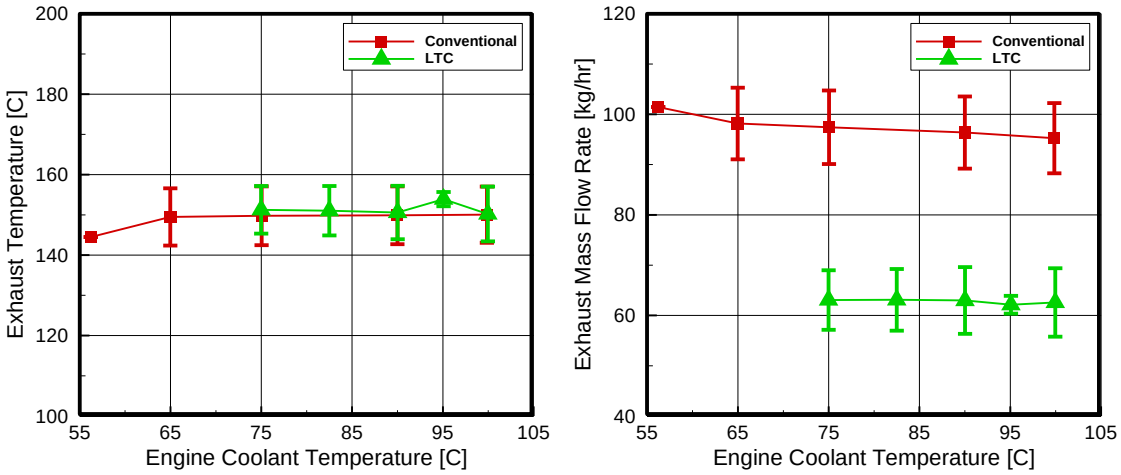

Figure 30. Post-turbocharger exhaust temperatures as a function of ECT

In contrast, the exhaust energy for LTC drops from a value above its conventional counterpart to a final value of 14% at an ECT of 100°C. The lower value at 100°C compared to conventional combustion is easily explained due to the large EGR rates which result in overall lower exhaust flow rates during LTC. However, exhaust temperature and flow rates do not change significantly across the LTC points, making the steep downward trend seem inexplicable. In fact, the sensible enthalpy portion of exhaust energy remains relatively constant as a function of ECT, as shown in Figure 31.

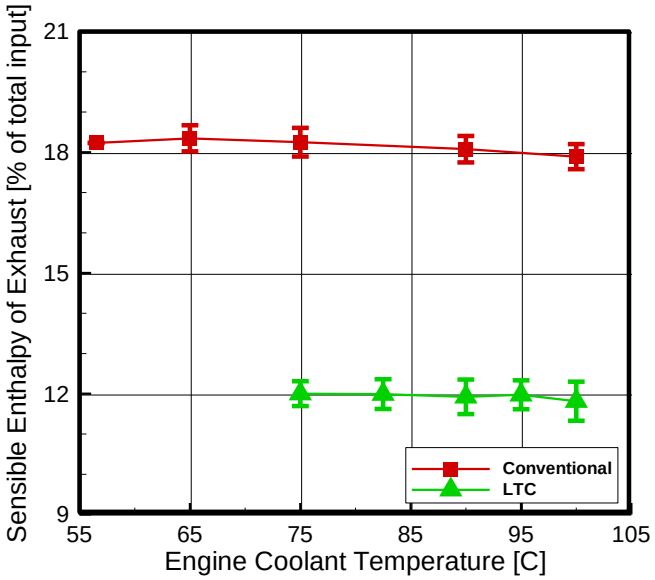

Figure 31. Percentage of input energy in sensible enthalpy of the exhaust as a function of ECT

However, the exhaust energy considers the thermal and chemical energy of the exhaust gases. Consequently, the large chemical energies of the products of incomplete combustion (CO and HC) significantly affect the average mixture energy of the exhaust despite their relatively small concentrations. Since these emissions drop steeply as a function of ECT (refer to Section 4.2.4), the overall exhaust energy corresponding decreases.

Surface heat transfer comprises an appreciable portion of the energy balance for the both the LTC and conventional conditions studied, as seen in Figure 32.

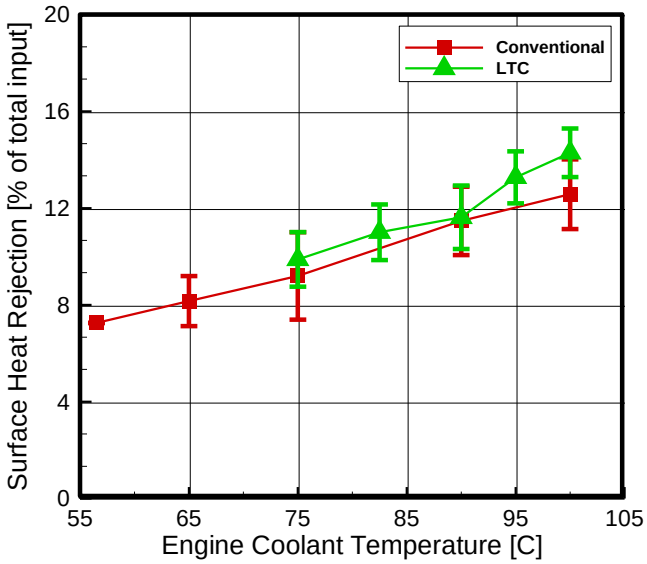

Figure 32. Percentage of input energy rejected by surface heat transfer as a function of ECT

Surface heat rejection for both LTC and conventional combustion increases with hotter ECTs which both testing conditions experiencing very similar values across the ECT range studied. The upward trend is simple to explain- higher coolant temperatures result in hotter engine surface temperatures which in turn result in larger convective and radiative heat transfer rates. The similar values for both LTC and conventional combustion also make sense because coolant temperatures should be the determining factor in surface temperature. While the LTC points are slightly higher, this is likely attributable to a minor rise in the surface temperatures of the turbocharger and EGR cooler thanks to engine boosting and EGR rates, respectively.

Surface heat transfer forming this non-negligible portion seems to run counter to conventional wisdom which asserts that brake power, coolant and exhaust each comprise a third of the input energy [6]; however, previous energy balance studies have found

similar results for surface heat transfer at low load conditions [29, 30, 46]. At higher loads, this surface term does in fact become fairly negligible, but this is only because surface heat transfer remains relatively constant while brake power, coolant heat rejection, and exhaust energy go up in significantly in magnitude thanks to the higher flow rates of fuel, air and coolant through the engine.

Last and least in its contribution to the energy balance is the charge air cooler (a.k.a. CAC or "intercooler"), depicted in Figure 33.

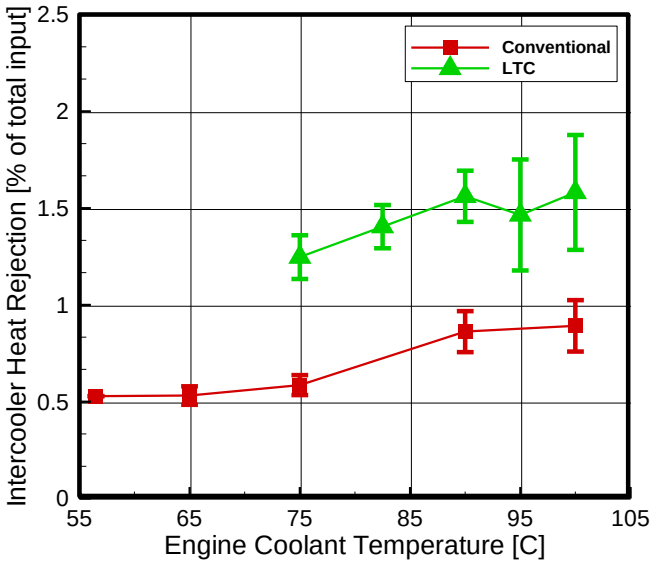

Figure 33. Percentage of input energy rejected by intercooler as a function of ECT

Unlike the conventional tests, low levels of boost are needed to provide the back pressure required for the high EGR rates in the LTC tests; consequently, the charge air enters the CAC at slightly higher pressures and temperatures for the LTC conditions. The larger temperature gradient between the air and cooling water results in increased heat rejection rates, and its contribution to the energy balance is higher. The marginal upward trend as a function of ECT for both conditions is likely due to higher block temperatures which would warm the air as it passes through the compressor of the

turbocharger. Similar to the boosting, this would correspondingly increase the heat transfer rates between the air and cooling water.

4.2.7. Summary of Important Results

Since the quantifiable improvements in LTC due to increased ECT are spread across numerous previous sections, Table 11 condenses the pertinent parameters and their improvement or degradation relative to the baseline condition of 90°C. Since an increase in ECT is used to apply LHR techniques, the values of the various parameters at the highest ECT studied (100°C) are tabulated.

Table 11. Change in LTC measurements due to increase of ECT to 100°C

Parameter [units]	**@ 90°C**	**@ 100°C**	**Absolute Change**	**Relative Change**
NO_X concentration [ppm]	42.2	62.6	20.4	48.3%
Filter Smoke Number [FSN]	0.032	0.086	0.054	169%
$BSNO_X$ [g/kW-h]	1.00	1.31	0.31	31.0%
Rel. Reduction of $BSNO_X$ [%]	91.6	88.8	-2.8	-3.1%
CO concentration [ppm]	2310	1520	-790	-34.2%
THC concentration [ppm]	509	309	-200	-39.3%
Combustion Efficiency [%]	94.7	96.7	2.0	2.1%
Brake Fuel Conversion Efficiency [%]	21.0	24.0	3	14.3%

4.2.8. Discussion

The results of the application of LHR techniques to LTC operation show quantifiable changes in the engine's behavior. In particular, all of the parameters of interest, namely exhaust emissions and engine efficiencies, display meaningful trends

across the range of ECTs studied. Additionally, the changes for LTC operation are generally more drastic than for conventional combustion, pointing to a higher sensitivity to alterations in ECT. Due to this higher responsiveness, there are distinct changes in the difference between LTC and conventional behavior for the same increase in ECT, as shown in Table 11. While desirable traits such as the reduction NO_X and PM emissions are lessened in magnitude, there are significant improvements in the undesirable side effects of CO and HC emissions as well combustion and brake thermal efficiencies.

5. SUMMARY AND CONCLUSIONS

The work undertaken for this study consisted of two distinct portions, each with its own methods and objectives. The first involved the alteration of injection timing and EGR rate in order to achieve LTC operation on a light-duty diesel engine. The second part applied a LHR technique of increased ECT to the conventional and LTC conditions identified by the first section in order to quantify how much the detrimental effects of LTC can be mitigated. In addition, an energy balance was applied to the engine during all the test points to establish the significance and validity of the LHR-LTC results

Through analysis of the exhaust concentrations of NO_X and PM, LTC operation was validated for the low load, low speed conditions studied. Several other trends typical of LTC operation were also observed, namely an increase in CO and HC emissions and a decrease in the engine's efficiency. The appearance of these auxiliary effects in the test results further solidified the assertion of LTC operations. Lastly, some discussion was undertaken to tie these behaviors to the observed alterations in the pressure and AHRR profiles.

In the second section, the effect of ECT alteration on numerous engine operating parameters was studied for a range of temperatures. NO_X and PM did increase as a result of the higher ECTs; however, the quantifiable criteria established to identify LTC operation were still met for most values of ECT. More importantly, the detrimental effects of LTC were improved by appreciable amounts by increasing ECT from its typical value of 90°C to 100°C. CO and HC emissions were decreased by 34% and 39%, respectively. In addition, both the combustion and brake fuel conversion efficiency of the LTC test points improved by 2% and 14%, respectively.

While there are risks and technical difficulties which must be addressed in order to operate the engine at higher temperatures, these results form a promising basis for further studies exploring a LHR-LTC concept. However, there is a great deal of work that still needs to be done. First, a better understanding of the long-term engine wear issues resulting from this operation is needed, particularly in the areas of piston rings and cylinder walls. Also, simulations and computational work would be helpful in

explaining the combustion behavior throughout the cylinder. Lastly, a more aggressive reduction of heat transfer by the addition of ceramic coatings to the engine surfaces should be undertaken to explore the limits of mitigating LTC's side effects.

REFERENCES

[1] DieselNet, 2009, "Emission Standards- United States- Cars and Light-Duty Trucks," Retrieved: September 25, 2012, http://www.dieselnet.com/standards/us/ld_t2.php.

[2] Henein, N. A., Kastury, K. N., and Bryzik, W., 2008, "Advanced Low Temperature Combustion (ALTC): Diesel Engine Performance, Fuel Economy and Emissions," SAE Technical Paper (2008-01-0652).

[3] Reddy, C. S., Domingo, N., and Graves, R. L., 1990, "Low Heat Rejection Engine Research Status: Where Do We Go from Here?," SAE Technical Paper (900620).

[4] Jaichandar, S., and Tamilporai, P., 2003, "Low Heat Rejection Engines - An Overview," SAE Technical Paper (2003-01-0405).

[5] Ban-Weiss, G. A., 2007, "A Numerical Investigation into the Anomalous Slight NOx Increase when Burning Biodiesel: a New (Old) Theory," Fuel Processing Technology, 88 (7), pp. 659-667.

[6] Heywood, J. B., 1988, Internal Combustion Engine Fundamentals, McGraw-Hill, Inc., New York.

[7] Turns, S. R., 2012, An Introduction to Combustion: Concepts and Applications, McGraw-Hill, New York.

[8] Jacobs, T., 2005, "Simultaneous Reduction of Nitric Oxide and Particulate Matter Emissions from a Light-Duty Diesel Engine using Combustion Development and Diesel Oxidation Catalyst," Ph.D, University of Michigan, Ann Arbor.

[9] Alriksson, M., and Dnebratt, I., 2006, "Low Temperature Combustion in a Heavy Duty Diesel Engine Using High Levels of EGR," SAE Technical Paper (2006-01-0075).

[10] Stanglmaier, R., and Roberts, C., 1999, "Homogeneous Charge Compression Ignition (HCCI): Benefits, Compromises, and Future Engine Applications," SAE Technical Paper Series (1999-01-3682).

[11] Epping, K., Aceves, S., Bechtold, R., and Dec, J., 2002, "The potential of HCCI combustion for high efficiency and low emissions," Powertrain and Fluid Systems Conference and Exhibition, SAE International, San Diego, California.

[12] Gray, A. W., and Ryan, T. W., 1997, "Homegeneous Charge Compression Ignition (HCCI) of Diesel Fuel," SAE Paper (971676).

[13] Mase, Y., Kawashima, J., Sato, T., and Eguchi, M., 1998, "Nissan's New Multivalve DI Diesel Engine Series," SAE Paper (981039).

[14] Hasegawa, R., and Yanagihara, H., 2003, "HCCI Combustion in DI Diesel Engine," SAE International (2003-01-0745).

[15] Iwabuchi, Y., Kawai, K., Shoji, T., and Takeda, Y., 1999, "Trial of New Concept Diesel Combustion System- Premixed Compression-Ignited Combustion," SAE Technical Paper (1999-01-0185).

[16] Kokjohn, S., Hanson, R., Splitter, D., and Reitz, R., 2009, "Experiments and Modeling of Dual-Fuel HCCI and PCCI Combustion using In-Cylinder Fuel Blending," SAE International (2009-01-2647).

[17] Curran, S., Prikhodko, V., Cho, K., Sluder, C., Parks, J., Wagner, R., Kokjohn, S., and Reitz, R., 2010, "In-Cylinder Fuel Blending of Gasoline/Diesel for Improved Efficiency and Lowest Possible Emissions on a Multi-Cylinder Light-Duty Diesel Engine," SAE International (2010-01-2206).

[18] Ashley, S., 2010, "Dual-fuel lab engines achieve high efficiencies, low emissions," Retrieved: January 29, 2014, http://www.sae.org/mags/aei/8388/.

[19] Caton, J. A., 2011, "Thermodynamic Advantages of Low Temperature Combustion (LTC) Engines Using Low Heat Rejection (LHR) Concepts," SAE International (2011-01-0312).

[20] Simescu, S., Ryan, T., Neely, G., Matheaus, A., and Surampudi, B., 2002, "Partial Pre-Mixed Combustion with Cooled and Uncooled EGR in a Heavy-Duty Diesel Engine," SAE Technical Paper (2002-01-0963).

[21] Havstad, P. H., Gervin, I. J., and Wade, W. R., 1986, "A Ceramic Insert Uncooled Diesel Engine," SAE Paper (860447).

[22] Wade, W. R., Havstad, P. H., Ounsted, E. J., Trinkler, F. H., and Garwin, I. J., 1984, "Fuel Economy Opportunities with an Uncooled DI Diesel Engine," ImechE/SAE, pp. 11-24.

[23] Thring, R. H., 1986, "Low Heat Rejection Engines," SAE Paper (860314).

[24] Miyairi, Y., Matsuhisa, T., Ozawa, T., Oikawa, H., and Nakashima, N., 1989, "Selective Heat Insulation of Combustion Chamber Walls for a DI Diesel Engine with Monolithic Ceramics," SAE Technical Paper (890141).

[25] Woschni, G., Spindler, W., and Kolesa, K., 1987, "Heat Insulation of Combustion Chamber Walls – A Measure to decrease the Fuel Consumption of I.C.Engines?," SAE Paper (870339).

[26] Cheng, W. K., Wong, V. W., and Gao, F., 1989, "Heat Transfer Measurement Comparisons in Insulated and Non-Insulated Diesel Engines," SAE Paper (890570).

[27] Dickey, D. W., 1989, "The Effect of Insulated Combustion Chamber Surfaces on Direct-Injected Diesel Engine Performance, Emissions and Combustion," SAE Technical Paper (890292).

[28] Taymaz, I., 2006, "An experimental study of energy balance in low heat rejection diesel engine," Energy, 31 (2–3), pp. 364-371.

[29] Donn, C., Zulehner, W., Ghebru, D., Spicher, U., and Honzen, M., 2011, "Experimental Heat Flux Analysis of an Automotive Diesel Engine in Steady-State Operation and During Warm-Up," SAE International.

[30] Singh, S., Garg, A., Gupta, A., and Permude, A., 2013, "Analysis of Thermal Balance of Diesel Engine and Identification of Scope for Waste Heat Recovery," SAE International.

[31] Burke, R., and Brace, C., 2010, "The Effects of Engine Thermal Conditions on Performance, Emissions and Fuel Consumption," SAE International.

[32] Bittle, J., Knight, B., and Jacobs, T., 2010, "Biodiesel Effects on Cycle-to-Cycle Variability of Combustion Characteristics in a Common-Rail Medium-Duty Diesel Engine," SAE Technical Paper (2010-01-0867).

[33] Incropera, F. P., Bergman, T. L., Lavine, A. S., and DeWitt, D. P., 2011, Fundamentals of Heat and Mass Transfer, Wiley & Sons, Inc, New York.

[34] Yang, C., Ma, P., Jing, F., and Tang, D., 2003, "Excess molar volumes, viscosities, and heat capacities for the mixtures of ethylene glycol+ water from 273.15 K to 353.15 K," Journal of Chemical & Engineering Data, 48 (4), pp. 836-840.

[35] Figliola, R., and Beasley, D., 2000, "Probability and Statistics," Theory And Design For Mechanical Measurements, J. Wiley & Sons, Inc., New York, pp. 109 – 148.

[36] Stivender, D. L., 1971, "Development of a fuel-based mass emission measurement procedure," International Mid-Year Meeting, SAE International, Montreal, Quebec, Canada.

[37] Storey, J., Lewis, S., West, B., Huff, S., Slucer, C., Wagner, R., Domingo, N., Thomas, J., and Kass, M., 2005, "Hydrocarbon species in the exhaust of diesel engines equipped with advanced emissions control devices," CRC project no. AVFL-10b-2.

[38] Bittle, J. A., 2010, "Two-stage ignition as an indicator of low temperature combustion in a late injection pre-mixed compression ignition control strategy," Master of Science Thesis, Texas A&M University, College Station, TX.

[39] Brunt, M., and Platts, K., 1999, "Calculation of heat release in direct injection diesel engines," SAE Transactions – Journal of Engines, 108, pp. 161-175.

[40] Foster, D. E., 1985, "An overview of zero-dimensional thermodynamic models for IC engine data analysis," SAE International Fall Fuels and Lubricants Meeting and Exhibition, Tulsa, Oklahoma.

[41] Depcik, C., Jacobs, T., Hagena, J., and Assanis, D., 2007, "Instructional use of a single-zone, premixed charge, spark-ignition engine heat release simulation," International Journal of Mechanical Engineering Education, 35 (1), pp. 1-31.

[42] National Aeronautics and Space Administration, 1993, "Coefficients for Calculating Thermodynamic and Transport Properties of Individual Species", By McBride, B., Gordon, S., and Reno, M., NASA Technical Memorandum 4513, Retrieved: March 10, 2014, Available at: http://ntrs.nasa.gov/archive/nasa/casi.ntrs.nasa.gov/19940013151.pdf

[43] DieselNet, 2010, "Gaseous Emissions- Nitrogen Oxides," Retrieved: April 14, 2014, http://www.dieselnet.com/tech/emi_gas.php.

[44] Ojeda, W., Kumar, R., Zoldak, P., and Espinosa, R., 2008, "Development of a Fuel Injection Strategy for Diesel," SAE World Congress, Detroit, Michigan USA.

[45] Held, F. R., Werblinski, T., Vogel, T., and Wensing, M., 2012, "Time and Spatially Resolved Measurements of the Interaction of Combusting Diesel Spray and Walls with Elevated Temperatures," SAE Int. J. Engines, 5 (4), pp. 1709-1716.

[46] Smith, L. A., Preston, W. H., Dowd, G., Taylor, O., and Wilkinson, K. M., 2009, "Application of a First Law Heat Balance Method to a Turbocharged Automotive Diesel Engine," SAE International (2009-01-2744).

APPENDIX A

UNCERTAINTY VALUES FOR ENERGY BALANCE

Table 12 displays the results of the uncertainty calculations for the energy balance for conventional combustion test conditions.

Table 12. Total uncertainty of energy balance for conventional combustion

ECT [°C]	**Day 1** [kW]	**Day 2** [kW]	**Average** [kW]	**Average percent of input energy** [%]
56.5	1.07	-	1.07	5.7
65	1.05	1.05	1.05	5.7
75	1.00	1.09	1.04	5.5
90	0.99	1.02	1.01	5.5
100	0.98	1.04	1.01	5.4

Table 13 displays the results of the uncertainty calculations for the energy balance for the LTC test conditions.

Table 13. Total uncertainty of energy balance for LTC

ECT [°C]	**Day 1** [kW]	**Day 2** [kW]	**Average** [kW]	**Average percent of input energy** [%]
75	1.04	1.07	1.06	5.5
82.5	1.07	1.08	1.08	5.7
90	1.03	1.04	1.04	5.5
95	1.06	1.19	1.13	6.1
100	1.07	1.12	1.09	5.9

APPENDIX B

DAY-TO-DAY VARIATION OF ENERGY BALANCE TERMS

Table 14 through Table 17 display the raw values for the energy balance terms for both conventional and LTC conditions for both days studied.

Table 14. Conventional combustion energy balance terms for Day 1

ECT [°C]	**Brake Work** [%]	**Exhaust** [%]	**Coolant** [%]	**Intercooler** [%]	**Surface** [%]	**Remainder** [%]
75	21.2	20.3	50.3	0.5	7.3	0.4
82.5	22.4	19.6	46.7	0.6	8.9	1.8
90	24.0	20.2	46.0	0.6	10.5	-1.3
95	25.5	19.9	42.5	0.8	12.5	-1.1
100	26.8	19.4	37.5	0.8	13.6	1.9

Table 15. Conventional combustion energy balance terms for Day 2

ECT [°C]	**Brake Work** [%]	**Exhaust** [%]	**Coolant** [%]	**Intercooler** [%]	**Surface** [%]	**Remainder** [%]
75	21.2	20.3	50.3	0.5	7.3	0.4
82.5	22.6	21.2	54.3	0.5	7.4	-6.0
90	23.6	18.9	46.0	0.5	7.9	3.1
95	25.7	19.9	46.5	0.9	10.5	-3.6
100	25.1	19.7	43.4	1.0	11.6	-0.6

Table 16. LTC energy balance terms for Day 1

ECT [°C]	Brake Work [%]	Exhaust [%]	Coolant [%]	Intercooler [%]	Surface [%]	Remainder [%]
75	10.4	20.9	49.1	1.3	10.7	7.6
82.5	16.1	17.3	49.9	1.5	11.8	3.4
90	21.6	15.0	47.5	1.7	12.6	1.7
95	22.0	13.1	45.8	1.3	14.0	3.7
100	23.7	13.3	44.6	1.4	15.0	2.1

Table 17. LTC energy balance terms for Day 2

ECT [°C]	Brake Work [%]	Exhaust [%]	Coolant [%]	Intercooler [%]	Surface [%]	Remainder [%]
75	11.1	22.1	52.1	1.2	9.1	4.5
82.5	16.7	18.3	52.0	1.3	10.2	1.4
90	20.6	15.6	50.9	1.5	10.7	0.8
95	23.4	15.4	51.8	1.7	12.5	-4.7
100	24.4	14.7	49.5	1.8	13.6	-3.9